



## RESEARCH ARTICLE

10.1029/2021JG006525

### Key Points:

- The drought-induced leaf area index changes in the land surface model JSBACH are improved and the resultant climate feedbacks are assessed
- Relative to the total drought effects, leaf shedding contributes 35% to the reduction in land carbon uptake and 12% to surface warming
- It is important for land surface models to incorporate drought deciduousness in tropical rainforests to improve future climate projections

### Supporting Information:

Supporting Information may be found in the online version of this article.

### Correspondence to:

H.-W. Wey,  
hao-wei.wei@mpimet.mpg.de



### Citation:

Wey, H.-W., Pongratz, J., Nabel, J. E. M. S., & Naudts, K. (2022). Effects of increased drought in Amazon forests under climate change: Separating the roles of canopy responses and soil moisture. *Journal of Geophysical Research: Biogeosciences*, 127, e2021JG006525. <https://doi.org/10.1029/2021JG006525>

Received 8 JUL 2021

Accepted 25 FEB 2022

# Effects of Increased Drought in Amazon Forests Under Climate Change: Separating the Roles of Canopy Responses and Soil Moisture

Hao-Wei Wey<sup>1,2,3</sup> , Julia Pongratz<sup>1,4</sup>, Julia E. M. S. Nabel<sup>1,5</sup> , and Kim Naudts<sup>1,6</sup> 

<sup>1</sup>Max Planck Institute for Meteorology, Hamburg, Germany, <sup>2</sup>International Max Planck Research School on Earth System Modelling, Hamburg, Germany, <sup>3</sup>Now at GEOMAR Helmholtz Centre for Ocean Research Kiel, Kiel, Germany, <sup>4</sup>Department of Geography, Ludwig Maximilian University of Munich, Munich, Germany, <sup>5</sup>Max Planck Institute for Biogeochemistry, Jena, Germany, <sup>6</sup>Department of Earth Sciences, Vrije Universiteit Amsterdam, Amsterdam, The Netherlands

**Abstract** The Amazon forests are one of the largest ecosystem carbon pools on Earth. Although more frequent and prolonged future droughts have been predicted, the impacts have remained largely uncertain, as most land surface models (LSMs) fail to capture the vegetation drought responses. In this study, the ability of the LSM JSBACH to simulate the drought responses of leaf area index (LAI) and leaf litter production in the Amazon forests is evaluated against artificial drought experiments. Based on the evaluation, improvements are implemented, including a dependency of leaf growth on leaf carbon allocation and a better representation of drought-dependent leaf shedding. The modified JSBACH is shown to capture the drought responses at two sites and across different regions of the basin. It is then coupled with an atmospheric model to simulate the carbon and biogeophysical feedbacks of drought under future climate. We separate the drought impacts into (a) the direct effect, resulting from drier soil and stomatal closure, which does not involve a change in canopy structure, and (b) the LAI effect, resulting from leaf shedding and involving canopy response. We show that the latter accounts for 35% of reduced land carbon uptake ( $9 \pm 10$  vs.  $26 \pm 7$  g/m<sup>2</sup>/yr; mean  $\pm$  1 sd) and 12% of surface warming ( $0.09 \pm 0.03$  vs.  $0.7 \pm 0.07$  K) during the late 21st century. A north-south dipole of precipitation change is found, which is largely attributable to the direct effect. The results highlight the importance of incorporating drought deciduousness of tropical rainforests in LSMs to better simulate land-atmosphere interactions in the future.

**Plain Language Summary** More frequent and prolonged droughts are expected in the Amazon region, but land surface models poorly simulate forest drought responses such as drought-induced leaf shedding. We improve the land surface model JSBACH by comparing the results of numerical simulations with observations from artificial drought experiments. To understand how much impact leaf shedding will have on climate in the future, we run numerical simulations and separate the climate effects into (a) the direct effect, caused by drying soil and the leaves closing their stomata (pores on the leaves regulating gas exchange), and (b) the effect of leaf shedding. The effect of leaf shedding contributes to 35% of the reduced absorption of CO<sub>2</sub> by land, and to 12% of surface warming. Rainfall increases in the north and decreases in the south mostly because of the direct effect of drought. In conclusion, it is important to correctly simulate leaf shedding to have more accurate predictions of future climate.

## 1. Introduction

Drought impacts plants by limiting soil moisture and has been predicted to become more frequent and prolonged in many places of the world, including the Amazon basin (Chadwick et al., 2015; Cook et al., 2020; Duffy et al., 2015; Joetjzer et al., 2013; Malhi et al., 2008). As the Amazon forests currently account for about a quarter of the natural carbon sink in global forests (Friedlingstein et al., 2019; Pan et al., 2011), it is important for carbon cycle and climate studies to understand how future soil drying will affect the Amazon forests. Generally, the responses of trees to water shortage contains several stages. In the short term, plants under drought conditions can save water by reducing transpiration through the physiological response of stomatal closure. Later, if low soil moisture persists, leaf shedding can occur and perturb the canopy structure. If the water shortage continues without relief, tree death will eventually take place, which will have large impacts on forest structure (Corlett, 2016).

© 2022. The Authors.

This is an open access article under the terms of the [Creative Commons Attribution License](https://creativecommons.org/licenses/by/4.0/), which permits use, distribution and reproduction in any medium, provided the original work is properly cited.

Several drought events have taken place in the Amazon since the beginning of the 21st century, including the years of 2005 and 2010. For both years, the drought has been attributed to the combination of El Niño and an anomalously warm tropical North Atlantic Ocean during the dry season (Lewis et al., 2011; Marengo et al., 2008; Zeng et al., 2008). From the two drought events in the Amazon, prominent effects on forests have been found by studies of both remote sensing-based and in situ observations. Measurements of LiDAR waveforms before and after 2005 showed a change in forest structure, which was related to a significant loss of carbon (Yang et al., 2018). The 2010 drought was also shown to have large impacts on the carbon budget in the Amazon. Atmospheric measurements suggested that considering the emission from fire, the Amazon was a carbon source of 0.5 PgC during the 2010 drought, instead of the usual close-to-neutral conditions during normal years (Gatti et al., 2014). In addition to the observations of past drought events, field-campaigns to artificially induce drought in the forest have also been conducted (Fisher et al., 2007; Meir et al., 2018; Nepstad et al., 2002). These artificial drought experiments can help us understand how trees react to drought at stand-level. At the same time, detailed information on soil and tree physiology is provided through intensive measurements to facilitate the investigation of mechanisms.

The observations at the artificial drought sites in the Amazon have enabled evaluations of model performances. Multi-model simulations have been conducted and when compared with the observations from the drought experiments, only a few models managed to capture the timing and magnitude of the responses, including leaf shedding, changes in autotrophic respiration ( $R_a$ ), and the enhanced mortality rate after several years of drought (Joetzer et al., 2014; Powell et al., 2013). Another multi-model study found similar drought and temperature responses of gross primary production (GPP) and ecosystem respiration across models. However, the consistent responses were due to a compensation from inconsistent leaf area index (LAI) and leaf-scale responses (Rowland et al., 2015). The inconsistency highlights the importance of separating leaf-scale physiological and canopy-scale LAI effects of drought. Another multi-model study assessed the ability of models to capture the seasonality of carbon fluxes in the Amazon. It was shown that the models tended to simulate a dry-season decline of GPP, in contrast to the observations. It was suggested that the importance of water limitation was overestimated in simulating the GPP seasonality, and the roles of biological processes such as leaf phenology were missing in the models (Restrepo-Coupe et al., 2017). Therefore, attention should be paid to improve our understanding on vegetation drought responses at different scales.

Despite the limited capacity of vegetation models, in order to understand the future climate effects of droughts, they are coupled with the atmospheric models as components of Earth System Models (ESMs) to account for land-atmosphere interactions in a warming and high-greenhouse-gas world. For instance, in the GLACE-CMIP5 experiment, simulations of an ensemble of ESMs were conducted with the aim to quantify the influences of soil moisture on climate and land-atmosphere interaction. By comparing results of the reference simulation and simulation with prescribed soil moisture at the level of the historical climatological mean (1971–2000), the effect of soil moisture is quantified. The GLACE-CMIP5 experiment has been applied to investigate the future influences of soil moisture in terms of biogeophysical effects (Berg et al., 2016; Lorenz et al., 2016; May et al., 2017; Zhou et al., 2019) and terrestrial carbon budget (Green et al., 2019; Humphrey et al., 2021). However, as the vegetation drought responses are not properly simulated by land surface models within the ESMs, results from the coupled model studies should be interpreted with caution. For example, the CMIP5 models have been shown to overestimate the responses of GPP and LAI to hydrological anomalies (Huang et al., 2016). Furthermore, it has been shown that soil moisture stress is a major source of carbon cycle uncertainty in ESM simulations, which is due to the overly simplified representation of the vegetation drought response in the land surface models within ESMs (Trugman et al., 2018). In order to reduce the uncertainty of future climate projections in the Amazon forests due to drought, it is therefore crucial to improve the simulated vegetation drought responses.

While previous multi-model studies have explored how well vegetation models capture artificial droughts in the Amazon, in this study, we use the land surface model JSBACH to explore improvements in representation of drought responses and assess their effects on land-atmosphere interaction. JSBACH has been actively contributing to different model intercomparison projects in both land-only and coupled configurations, and has been shown to reasonably simulate the carbon budget of land sink and land-use change among other land surface models (Friedlingstein et al., 2019). However, the vegetation drought responses of JSBACH have not been evaluated in previous studies. Here, we implement modifications to improve JSBACH based on the artificial drought experiments in the eastern Amazon and evaluate the performance of the model both at site-level and across the Amazon basin. We aim to address the drought responses in moist tropical forest at the time scale of episodic

to multiyear droughts, which are caused by ENSO events or anomalous warm sea surface temperature in the North Atlantic, and at a similar time scale as the artificial drought experiments (see e.g., Janssen et al., 2020, for a discussion on different types of droughts). Moreover, as previous studies have pointed out the importance of separating vegetation drought responses at different scales, we separate the forest drought responses and their feedback to the atmosphere into (a) the direct effect, which results from drier soil and stomatal closure and does not involve a change in LAI, and (b) the LAI effect, which is a result of leaf shedding due to drought and thus perturbs the canopy structure. The separation of the environmental control and stomatal response as a direct effect and leaf phenology as part of an indirect effect has also been used in previous studies (Flack-Prain et al., 2019; Wu, Guan, et al., 2017). For the first time, an estimate of the respective contributions from the direct and LAI effects on carbon budget components and biogeophysical effects under future climate is provided, in order to improve our understanding of their importances in the Amazon forests.

## 2. Methodology

### 2.1. Site Description

We utilize data from the two ecosystem-scale throughfall exclusion (TFE) experiments carried out in the eastern Amazon forests (Fisher et al., 2007; Nepstad et al., 2002). The TFE experiments are composed of two 1-ha ( $100 \times 100$  m) plots: the controlled (CTR) and the experimental (EXP) plots. At the EXP plot, the soil moisture is artificially reduced by deflecting away about 50% of the throughfall (rainfall penetrating the canopy) with drainage structures installed 1–2 m above the forest floor. The two TFE experimental sites are at Tapajós National Forest (TAP) and Caxiuanã National Forest (CAX), both in the Brazilian state of Pará. The annual precipitation at both sites is 2,000–2,300 mm, with clear seasonality and wet season roughly between December and June. The soil at TAP is more clay-rich and deeper (60%–80%; >100 m), and the soil at CAX is sandier (70%–83% sand) with a shallower water table at 15–20 m. At TAP, the experiment ran from 2000 to 2006, with the throughfall excluded only during the wet seasons. At CAX, the experiment started in 2001 and continued for at least 16 years, with the throughfall excluded all year round. Comprehensive measurements were conducted at the sites at both CTR and EXP plots, including LAI, soil moisture at different depths, diameter at breast height, which is used to derive aboveground biomass, and coarse and fine litter produced from stems, twigs, leaves, fruits and flowers of the trees.

To understand how well JSBACH can reproduce the observations at the TFE experimental sites, we conduct land-only (also known as offline) simulations at the TFE experimental sites. Two sets of simulations are conducted. One set is with precipitation kept unchanged (CTR), and the other with precipitation reduced to 50% of the original value (EXP; at TAP only during wet season from January to June and all-year round at CAX). (See Text S1 in Supporting Information S1 for details of offline simulations.)

### 2.2. Moderate-Resolution Imaging Spectroradiometer (MODIS) LAI

To evaluate the model performance at the scale of the Amazon basin, we use the LAI data from MODIS. We use both the 500 m resolution product of MOD15A2H MODIS/Terra Leaf Area Index/FPAR 8-Day L4 Global 500 m SIN Grid V006 (Myneni et al., 2015), and the global gridded product at  $0.5^\circ$  resolution, both derived by the Integrated Climate Data Center of the University of Hamburg (Kern, 2021).

For site-level comparison, the 500 m resolution product is used and the data is retrieved from the nearest grid point in the h12v09 tile. For comparisons at regional scale, the  $0.5^\circ$  product is used. For both products, we discard data derived not from the main algorithm but from the empirical algorithm. However, saturation is still possible, as clouds might be present or clear sky was assumed (Kern, 2021). To analyze the regional patterns, the Amazon basin is divided into the Northern Amazon (NA,  $70^\circ\text{W}$ – $55^\circ\text{W}$ ,  $5^\circ\text{S}$ – $5^\circ\text{N}$ ) and the Southern Amazon (SA,  $70^\circ\text{W}$ – $50^\circ\text{W}$ ,  $15^\circ\text{S}$ – $5^\circ\text{S}$ ). Additionally, the Northwestern Amazon (NWA,  $75^\circ\text{W}$ – $60^\circ\text{W}$ ,  $10^\circ\text{S}$ – $5^\circ\text{N}$ ), where the rainfall seasonality is weaker than the rest of the Amazon basin, is also considered (Yin et al., 2013, see Figure 5 for locations of the regions).

### 2.3. Model Description and Modifications

The baseline model utilized in this study is the forest management (FOM) branch of the land surface model JSBACH v3.2 (hereafter the standard JSBACH; Reick et al., 2021). JSBACH is the land component of the Max Planck Institute Earth System Model (MPI-ESM; Mauritsen et al., 2019). However, JSBACH can also be run alone in offline mode with meteorological data as forcing. A full description of JSBACH is given in Reick et al. (2021). In this section, we briefly introduce the processes related to vegetation drought responses. First, we describe how stomatal conductance responds to soil moisture stress in JSBACH, which is not modified in this study and kept the same in both the standard and modified JSBACH. We then describe the formulation of LAI and leaf litter production in the standard JSBACH and the modification implemented to the model within this study.

#### 2.3.1. Stomatal Conductance Under Water Stress

In JSBACH, the stomatal conductance under water stress is calculated from the unstressed stomatal conductance via a simple scaling factor  $f_{ws}$  based on the following equation:

$$f_{ws} = \begin{cases} 0, & \text{for } W \leq W_{wilt} \\ \frac{W - W_{wilt}}{W_{crit} - W_{wilt}}, & \text{for } W_{wilt} < W < W_{crit} \\ 1, & \text{otherwise,} \end{cases} \quad (1)$$

where  $W$  is the amount of soil water,  $W_{crit} = 0.75 \cdot W_{max}$ ,  $W_{wilt} = 0.35 \cdot W_{max}$ , and  $W_{max}$  is the maximum water storage, all calculated within root zone and in the unit of water depth.

The stomatal conductance under water stress  $g_{C, stress}^{H_2O}$  is therefore related to the unstressed stomatal conductance  $g_C^{H_2O}$  following Equation 2:

$$g_{C, stress}^{H_2O} = \begin{cases} f_{ws} \cdot g_C^{H_2O}, & \text{for } q_a \leq q_s \\ 0, & \text{otherwise,} \end{cases} \quad (2)$$

where  $q_a$  is specific humidity of the lowest atmospheric layer, and  $q_s$  is saturation humidity at the surface, calculated from surface temperature and surface pressure.

#### 2.3.2. LAI

##### 2.3.2.1. Standard JSBACH

While more details on how JSBACH simulates leaf phenology are provided in Reick et al. (2021), we describe here the parts that are essential for our study. The LAI is governed in JSBACH by the phenology module, in which the leaf dynamics are a combination of logistic growth and exponential decay. The growth and shedding of leaves are based on the following equation:

$$\frac{d\Lambda}{dt} = k\Lambda \left( 1 - \frac{\Lambda}{\Lambda_{max}} \right) - p\Lambda \quad (3)$$

where  $\Lambda$  is LAI,  $\Lambda_{max}$  is the maximum LAI that can be supported by the plant, and  $k$  and  $p$  are phenological parameters, representing the growth and shedding rate of leaves, respectively. In the FOM branch of JSBACH used in this study, the maximum LAI depends on the available leaf biomass (see Nabel et al., 2020, and reference therein).

The different plant functional types (PFTs) in JSBACH are categorized into five phenological types. According to the phenological types, the conditions of how the phenological parameters  $k$  and  $p$  change are different. Multiple PFTs can be classified as the same phenological type. In this study, we focus on the leaf phenology in the Amazon forests, which is represented in JSBACH predominately by tropical evergreen trees and represented by



the raingreen phenology. Other PFTs represented by the raingreen phenology include tropical deciduous trees and raingreen shrubs.

For the raingreen phenology, three different conditions are distinguished when determining the phenological parameters  $k$  and  $p$ . In the first condition, if the relative soil moisture (defined as soil moisture divided by field capacity) in the root zone  $w$  is greater than the wilting point  $w_{\text{wilt}}$ , and the net primary production (NPP) is positive, the phenological parameters  $k$  and  $p$  are determined as follows:

$$k = k_{\text{growth}}$$

$$p = p_{\text{aging}} + k_{\text{growth}} \begin{cases} 0, & \text{for } w_{\text{crit}} \leq w \\ \frac{w_{\text{crit}} - w}{w_{\text{crit}} - w_{\text{wilt}}}, & \text{for } w_{\text{wilt}} < w < w_{\text{crit}}, \end{cases} \quad (4)$$

where the critical soil moisture  $w_{\text{crit}}$  is 0.65,  $w_{\text{wilt}}$  is 0.35, both in relative soil moisture.  $p_{\text{aging}}$  is 0.005 and  $k_{\text{growth}}$  is 0.08. We note that because of the existence of the threshold  $w_{\text{crit}}$ , there is no difference in leaf growth whether the relative soil moisture is 0.65 or 1. Also the wilting point is universally set to 0.35, which does not consider local soil or vegetation properties.

In the second condition, if  $w$  is less than or equal to  $w_{\text{wilt}}$ ,  $k$  and  $p$  are determined as:

$$k = 0$$

$$p = p_{\text{dry}}, \quad (5)$$

where  $p_{\text{dry}}$  is 0.12.

Finally, in the third condition, if  $w$  is greater than  $w_{\text{crit}}$  but NPP is not positive, LAI will not be updated.

### 2.3.2.2. Modifications

Several modifications are implemented to the leaf dynamics (see Section 4.1 in discussion for the rationale of the modifications). First of all, the three different conditions are reduced to only one equation. In addition, the threshold for LAI to respond to water stress is removed via setting  $w_{\text{crit}}$  to 1. In the standard JSBACH, the wilting point  $w_{\text{wilt}}$  is assigned with a global invariant value, which is replaced with a global map with spatial variation to incorporate soil and vegetation properties locally (Patterson, 1990). The growth rate is now proportional to the NPP input to represent the carbon allocation to leaves. Finally, the shedding rate is now decoupled from the growth rate and a new parameter  $p_{\text{stress}}$  is created to represent the component of shedding rate that is determined by water stress.

The following equations summarize the phenological parameters  $k^*$  and  $p^*$  in the modified JSBACH:

$$k^* = NPP \cdot k_{\text{growth}}$$

$$p^* = p_{\text{aging}} + p_{\text{stress}} \begin{cases} \frac{w_{\text{crit}} - w}{w_{\text{crit}} - w_{\text{wilt}}}, & \text{for } w_{\text{wilt}} < w \leq w_{\text{crit}} = 1 \\ 1, & \text{for } w \leq w_{\text{wilt}} \end{cases} \quad (6)$$

Plugging the parameters  $k^*$  and  $p^*$  into the phenology equation (Equation 3) results in the following equation:

$$\frac{d\Lambda}{dt} = NPP \cdot k_{\text{growth}} \cdot \Lambda \left( 1 - \frac{\Lambda}{\Lambda_{\text{max}}} \right) - [p_{\text{aging}} + p_{\text{stress}} \cdot \beta] \cdot \Lambda \quad (7)$$

where:

$$\beta = \begin{cases} \frac{1 - w}{1 - w_{\text{wilt}}}, & \text{for } w_{\text{wilt}} < w \leq 1 \\ 1, & \text{for } w \leq w_{\text{wilt}} \end{cases}$$

There are three tunable parameters ( $k_{\text{growth}}$ ,  $p_{\text{aging}}$  and  $p_{\text{stress}}$ ) in the modified JSBACH, and we choose the parameter set that gives the best results simulating LAI at EXP plot at TAP for the first two years of the experiment. The choice of TAP as the site for tuning is because concurrent comprehensive measurements of both soil moisture and LAI are only available at TAP (LAI was only measured every six months during the experiments at CAX). The usage of data only for the first two years (2000 and 2001) at EXP plot is because after two years, the effects of enhanced mortality have already manifested, which affect the LAI and litter production (Brando et al., 2008). As a drought-dependent tree mortality has not been implemented in JSBACH, the model is not tuned against the data after two years. (See Figure S1 in Supporting Information S1 for the Taylor diagram for the tuning process.)

### 2.3.3. Leaf Litter Production

In JSBACH, the carbon of leaves is stored in the so-called green pool, which is composed of leaves as well as fine roots and vascular tissues. Therefore, the carbon lost due to leaf shedding is removed from the green pool. Changes in the size of the green pool are described by the following equation (under conditions of no nitrogen limitation):

$$\frac{dC_G}{dt} = NPP_{\text{PG}} - F_{\text{litter}} - F_{\text{grazing}}, \quad (8)$$

where  $C_G$  is green pool size,  $NPP_{\text{PG}}$  is NPP allocated to the green pool,  $F_{\text{litter}}$  is green litter flux (litter produced from leaves, fine roots, and vascular tissues) and  $F_{\text{grazing}}$  is carbon loss due to grazing.

In the standard JSBACH,  $F_{\text{litter}}$  is given by the following equation:

$$F_{\text{litter}} = \frac{\gamma_G}{SLA} \cdot \max\left(r_{\text{shed}} \cdot \Lambda, -\frac{d\Lambda}{dt}\right), \quad (9)$$

where  $\gamma_G$  is the ratio of size of leaves to size of total green pool and assumed as a constant of 4; SLA (specific leaf area) and  $r_{\text{shed}}$  (inverse leaf longevity) are PFT-dependent parameters.  $r_{\text{shed}} \cdot \Lambda$  represents the litter production due to aging, and  $-\frac{d\Lambda}{dt}$  represents the litter production due to water stress.

Equation 9 shows that, in the standard JSBACH, green litter is produced either at the pre-defined aging rate or net change rate of LAI, when it is larger than the aging process. Therefore, the green litter production is dependent only on current LAI or the net change of LAI, and is decoupled from the shedding rate used in the phenology equation (Equation 3).

Modifications are thus also implemented to the formulation of green litter production. Since leaves are both grown and shed simultaneously, the dependence of leaf litter production on net LAI change is replaced, and the litter production now accounts directly for the shed part of leaves. In addition, the ratio of green litter to leaf litter ( $\gamma_G$ ) is updated according to estimates from Girardin et al. (2016). The green litter production now follows the equation:

$$F_{\text{litter}} = \frac{\gamma_G}{SLA} \cdot p\Lambda, \quad (10)$$

with  $\gamma_G$  updated from 4 to 2, and  $p$  is the shedding rate taken from Equation 6.

### 2.4. Design of Coupled Experiments

To investigate the climatic effects of the responses of the Amazon forests to future drought, the atmosphere as well as terrestrial ecosystem should be considered together. Therefore, we conduct a series of land-atmosphere coupled simulations, where JSBACH is coupled with the atmospheric general circulation model ECHAM6 (or equivalently, the MPI-ESM is run in an AMIP-type configuration). The model utilized is based on the official CMIP6 version of the MPI-ESM (See Text S2 in Supporting Information S1 for information on the model version).

In the AMIP-type configuration, the sea surface temperature and sea ice concentration are prescribed as the boundary condition. The sea surface temperature and sea ice concentration are calculated by combining the trend during the 21st century under the RCP8.5 scenario simulated by MPI-ESM (Mauritsen et al., 2019) and the spatial pattern from HadISST (Rayner et al., 2003; See Text S3 in Supporting Information S1 for the detail of the

**Table 1**  
*Design of the Coupled Experiments*

Experiment name	GHG forcing	Soil moisture	LAI	LAI response to future GHG forcing	LAI response to future water stress
21sm-21L	RCP8.5	Interactive	Interactive	✓	✓
20sm-20L	RCP8.5	1971–2000 climatology	Interactive	✓	
21sm-20L	RCP8.5	Prescribed from 21sm-21L	Prescribed from 20sm-20L	✓	

*Note.* In 20sm-20L, the soil moisture is prescribed with the 1971–2000 climatology and the LAI is interactive. In 21sm-20L, the soil moisture is prescribed according to 21sm-21L and the LAI is prescribed from 20sm-20L. The difference between 21sm-20L and 20sm-20L reveals the direct effect of drought from soil moisture and stomatal closure alone. The difference between 21sm-21L and 21sm-20L reveals the LAI effect of drought from the LAI reduction due to drier soil. See Figure 1 for a summary about the direct and LAI effects. The experiments are run with both the standard and modified JSBACH. For each experiment, five ensemble members are conducted with different initial date. 21sm-21L (sm: soil moisture; L: LAI) is the reference experiment where both the soil moisture and LAI are interactive.

calculation). As we focus on the response of intact forests, anthropogenic land use and land cover change are not considered. We use a static land use and land cover map for the year 2010 from the TRENDY v7 simulation by JSBACH (Le Quéré et al., 2018; Sitch et al., 2015). In JSBACH, most of the vegetation in the Amazon belongs to the tropical evergreen PFT, with a small portion being raingreen shrubs over eastern Brazil (See Text S4 in Supporting Information S1 for a comparison of the trait values of the tropical evergreen PFT with field measurements). Both of the PFTs belong to the raingreen phenology in JSBACH and are thus subject to the modifications described in Section 2.3. (See Figure S2 in Supporting Information S1 for the cover fraction of different PFTs simulated in the experiments.)

The design of the experiment set is described below, and a summary is provided in Table 1. With the configuration and boundary conditions described above, the model is run with pre-industrial forcing for several hundred years, until the global soil carbon reaches equilibrium. After reaching equilibrium, the simulation is run with historical forcing from 1850 to 2014. We then perform a set of future simulations. A reference simulation starts from 2015, with the business-as-usual RCP8.5 scenario as the greenhouse gas (GHG) forcing, and both soil moisture and LAI are interactive. The simulation is called “21st-century-soil-moisture-21st-century-LAI”, denoted as 21sm-21L. Since the LAI is regulated both by soil moisture (which is expected to be lower in the future) and available carbon allocated to the leaves (which, due to future higher CO<sub>2</sub> concentration, is presumably higher in the future), the LAI in 21sm-21L includes the effects of both future GHG forcing and future water stress.

For the first experimental simulation, the same forcing is used as the reference simulation (i.e., 21sm-21L). However, the soil moisture is prescribed according to the daily climatology from the historical simulation during 1971–2000, and the LAI is interactive. The LAI in this simulation therefore considers only future GHG forcing, but the effects from future soil drying are excluded, and therefore this simulation is called “20th-century-soil-moisture-20th-century-LAI”, or 20sm-20L.

Finally, in the second experimental simulation, the soil moisture is prescribed from the reference simulation 21sm-21L, and the LAI is prescribed from the experimental simulation 20sm-20L. The second experimental simulation is denoted as 21sm-20L (21st-century-soil-moisture-20th-century-LAI).

As shown in the schematic diagram in Figure 1, under future climate where drought conditions are enhanced due to GHG forcing, the climate is affected simultaneously by GHG forcing as well as the resultant drought forcing of lower soil moisture and LAI. To separate the direct effect (resulting from soil drying and stomatal closure and not involving changes in LAI) and the LAI effect (resulting from changes in LAI), we compare the results between different simulations. The comparison between 21sm-20L and 20sm-20L quantifies the direct effect, as the only difference between the simulations is the soil drying due to future GHG forcing. As the soil moisture in 21sm-21L experiment is fully interactive and contains the feedback of LAI on soil moisture, the negative feedback that LAI reduction can alleviate soil moisture drought is also included as part of the direct effect. (The LAI feedback is estimated to be an order of magnitude smaller than the pure direct effect without feedback. See Text S5 in Supporting Information S1 for details.) Similarly, the comparison between 21sm-21L and 21sm-20L quantifies the LAI effect, as the only difference between the simulations is the change in LAI due to future soil drying. As in all simulations, the GHG forcing is identical (RCP8.5), differences between the simulations therefore largely cancel out the warming and other climatic effects caused by the GHG forcing.

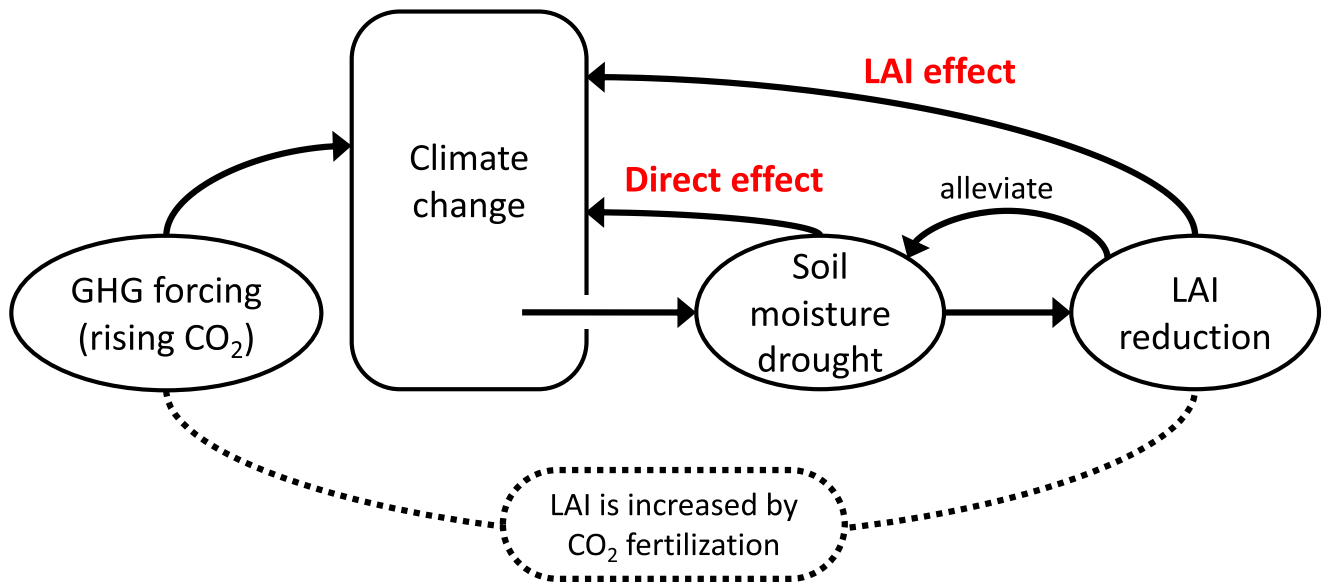


**Figure 1.** A schematic illustration of the focus of this study. The greenhouse gas (GHG) forcing of rising CO<sub>2</sub> changes the climate, with enhanced soil moisture drought as one of the signals. The enhanced soil moisture drought in turn results in leaf area index (LAI) reduction. LAI reduction alleviates the soil moisture drought as it reduces the loss of soil moisture via transpiration from plants. Meanwhile, LAI is also increased by GHG forcing as a result of the CO<sub>2</sub> fertilization effect. The direct effect of drought is the direct result of reduced soil moisture and associated stomatal response due to drought; the LAI effect of drought is the result of reduced LAI, which is due to the reduced soil moisture from drought. The focus of this study is to separate the roles of soil moisture (the direct effect) and canopy (the LAI effect) of drought responses. The effect of LAI feedback on soil moisture is considered in this study as part of the direct effect. See text for more details.

The simulations are conducted with both the standard and modified JSBACH as the land surface model. The simulations are run globally with a spatial resolution of T63 (ca. 200 km). For both versions, simulations of five ensemble members are conducted. The different ensemble members are produced by starting the historical simulation from different years of the pre-industrial simulations.

### 3. Results

#### 3.1. Model Evaluation Against In Situ and Remote-Sensing Data

The observed and simulated soil moisture, LAI, and leaf litter production at TAP are shown in Figure 2. The soil parameters in the two simulations are the same. However, for the two model versions, two spin-up simulations for reaching equilibrium were conducted respectively. Therefore, the soil moisture at the beginning between the two versions is different. For the standard JSBACH, the simulated LAI shows several features that do not match the observations (Figure 2, middle row of upper panel). At the CTR plot, the simulated LAI remains at a constant value without any variability, except for the drastic decrease (about 3 m<sup>2</sup>/m<sup>2</sup>) during the end of 2002 and 2003, which both do not exist in observations. At the EXP plot, the simulated LAI is either at the same value as the CTR plot, or drops to a low value that is never observed during the experiment period (by about 3 m<sup>2</sup>/m<sup>2</sup>; the lowest value at EXP plot in observation is about 4 m<sup>2</sup>/m<sup>2</sup>). At both CTR and EXP plots, a threshold behavior thus exists so that the simulated LAI remains at a constant value until soil moisture is below a specific level (about 0.23 m<sup>3</sup>/m<sup>3</sup>). When below this level, LAI evolves with time, but the decrease and recovery are both much faster compared with the observations. The features are improved in the modified JSBACH (Figure 2, middle row of lower panel). The simulated LAI at both plots have now gentle variability, with the standard deviation reduced for 0.4 m<sup>2</sup>/m<sup>2</sup> and 1.1 m<sup>2</sup>/m<sup>2</sup>, respectively. The response to drought at EXP plot is captured, with the correlation with the observations largely improved. The high biases at both CTR and EXP plots are also reduced (see Table 2 for a detailed comparison of simulated results between the two versions).

The improvement of the threshold behavior is clearly seen when we look at the relation between soil moisture and LAI. Figure 3 shows the concurrent soil moisture and LAI at the EXP plot of the observations and simulations for the whole experimental period. In the observations, the soil moisture and LAI have a moderate linear correlation ( $r = 0.519$ ). With a reduction of relative soil moisture (calculated as volumetric soil moisture divided by field

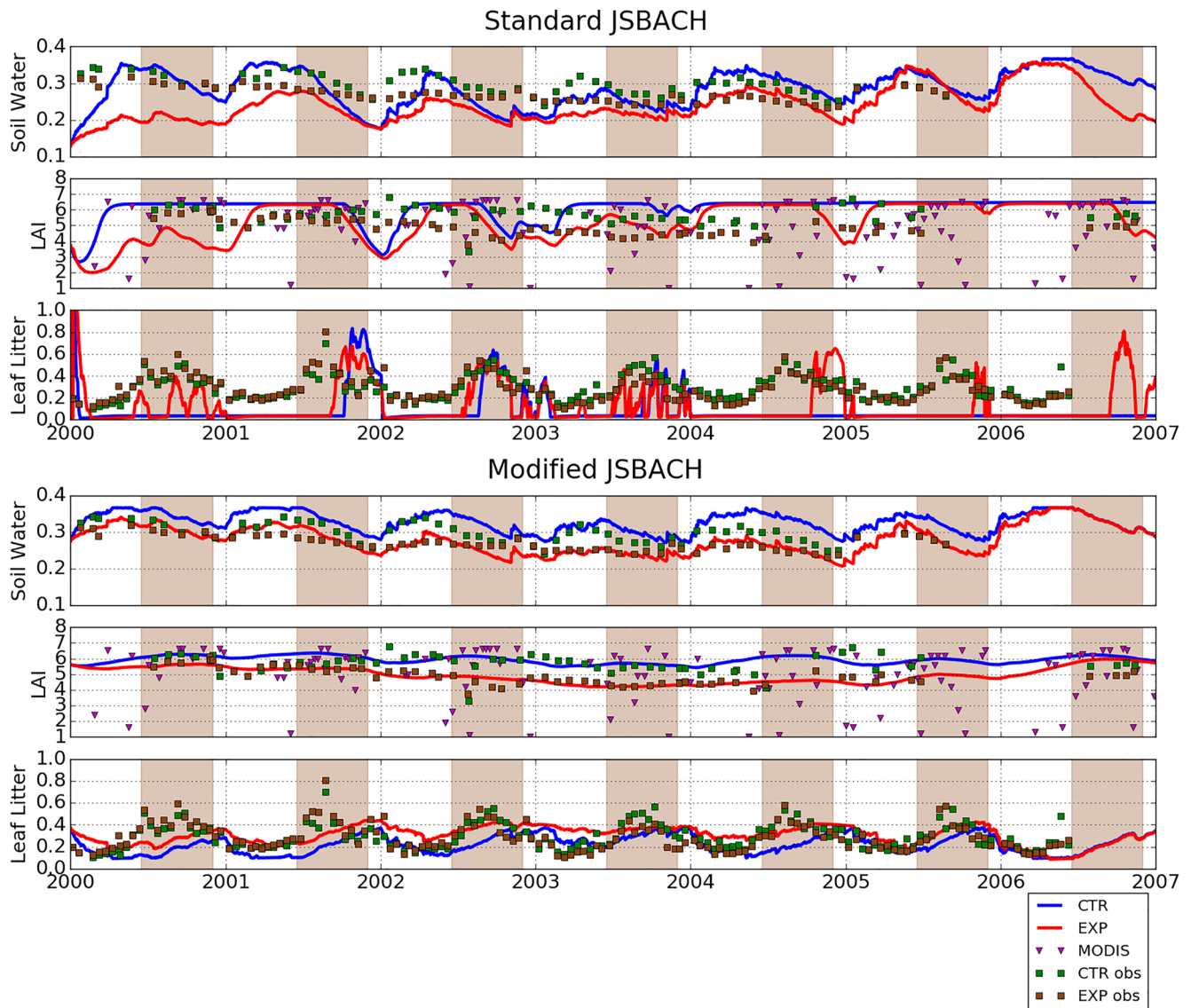


**Figure 2.** Time evolution of soil moisture (top of both panels;  $\text{m}^3/\text{m}^3$ ), leaf area index (LAI; middle of both panels;  $\text{m}^2/\text{m}^2$ ), and leaf litter production (bottom of both panels;  $\text{kg}/\text{m}^2/\text{yr}$ ) of both observations and simulations at the throughfall exclusion experimental site at Tapajós National Forest. (Top) standard (bottom) modified JSBACH. Two spin-up simulations for reaching equilibrium were conducted for the two model versions respectively, and therefore the initial soil moisture at 2000 is different. CTR: control plot; EXP: experimental plot (with throughfall exclusion); Dots: in situ observations; Triangles in magenta: MODIS LAI; Lines: simulations. Shading: dry seasons.

capacity) from about 0.9 to 0.7, the LAI changes from about 5.5 to 4.5 (Figure 3a). In the standard JSBACH, the LAI does not change at all when relative soil moisture is above 0.65, and the slope of change when relative soil moisture is below 0.65 is also too high. The linear correlation is also stronger than in the observations ( $r = 0.831$ ), indicating a too-strong control of soil moisture on LAI (Figure 3b). In the modified JSBACH, the threshold behavior is removed and the steep slope is improved. The linear correlation is still overestimated but reduces to a value closer to the observation ( $r = 0.702$ ; Figure 3c). While the linear correlation between observed soil moisture and LAI at EXP plot is moderate, the correlation of differences in LAI and soil moisture ( $\Delta\text{LAI}$  and  $\Delta[\text{soil moisture}]$ ) between EXP and CTR plots is poor (Figure S3 in Supporting Information S1), which indicates that LAI is not a simple function of current soil moisture but also depends on other factors such as the NPP input. The inclusion of NPP input in determining LAI growth in the modified JSBACH could thus help explain the improvement in the relationship between soil moisture and LAI shown in Figure 3.



**Table 2**  
*Comparison Between the Standard and Modified Version of JSBACH at Tapajós National Forest*

Variable	Plot	Version	Bias	dSDev	CRMSD	CCoef
LAI	CTR	Standard <sup>a</sup>	0.375	<b>0.102</b>	0.984	<b>−0.273</b>
		Modified <sup>a</sup>	<b>0.225</b>	−0.299	<b>0.628</b>	<i>−0.015</i>
	EXP	Standard <sup>b</sup>	−0.611	0.864	1.286	<i>−0.154</i>
		Modified <sup>b</sup>	<b>−0.070</b>	<b>−0.195</b>	<b>0.242</b>	<b>0.769</b>
Leaf litter	CTR	Standard <sup>c</sup>	−0.214	0.043	0.183	<i>0.124</i>
		Standard <sup>c,e</sup>	−0.222 <sup>a</sup>	0.022 <sup>a</sup>	0.151 <sup>a</sup>	0.291 <sup>a</sup>
		Modified <sup>c</sup>	−0.081	<b>−0.030</b>	0.119	0.313
		Modified <sup>c,e</sup>	<b>−0.080<sup>a</sup></b>	−0.031 <sup>a</sup>	<b>0.087<sup>a</sup></b>	<b>0.655<sup>a</sup></b>
	EXP	Standard <sup>d</sup>	−0.181	0.063	0.230	<i>0.104</i>
		Standard <sup>d,e</sup>	−0.198 <sup>a</sup>	<b>0.037<sup>a</sup></b>	0.146 <sup>a</sup>	0.583 <sup>a</sup>
		Modified <sup>d</sup>	−0.048	−0.066	0.140	<i>0.214</i>
		Modified <sup>d,e</sup>	<b>−0.035<sup>a</sup></b>	−0.063 <sup>a</sup>	<b>0.100<sup>a</sup></b>	<b>0.704<sup>a</sup></b>

*Note.* At the control plot (CTR), data from all years are used for calculation, while at the experimental plot (with throughfall exclusion; EXP), only data from the first 2 years are used. Values in bold indicate that the respective model version performs better than its counterpart. Values in italic indicate that the correlation is insignificant ( $p > 0.1$ ). Shown are the simulated bias, differences of standard deviation between simulations and observations (dSDev), centered root-mean-square differences (CRMSD), and correlation coefficient with observations (CCoef).

<sup>a</sup> $n = 59$ . <sup>b</sup> $n = 19$ . <sup>c</sup> $n = 154$ . <sup>d</sup> $n = 48$ . <sup>e</sup>Calculated with a lag of 90 days for the simulations.

In Figures 2 and 4, the MODIS LAI at 500 m resolution is also included for comparison with both the in situ observations and the simulations. However, while the maximum values of LAI within the year do not differ a lot between the in situ observations and MODIS data, the MODIS LAI is shown to have unrealistically large intra-year variations compared to the in situ data. Consistently, it has been pointed out in previous studies that the seasonal variation of MODIS does not match with in situ observations (e.g., Doughty & Goulden, 2008). Therefore, for evaluating drought responses at the TFE sites, we focus on the comparison between simulated and in situ observed LAI, and use the MODIS data only at the scale of the Amazon basin and over longer time periods.

The observed and simulated leaf litter production at TAP are shown in the bottom rows of the both panels in Figure 2. As in the comparison of LAI, the standard JSBACH also simulates the leaf litter production with features not seen in the observations (Figure 2, bottom row of upper panel). In the standard JSBACH, the production of leaf litter remains at low values close to zero for long stretches of time, with intermittent pulse-like jumps to high values. In comparison, the modified JSBACH simulates the leaf litter production with more appropriate magnitude and fewer biases (Figure 2, bottom row of lower panel). Although the magnitude and bias is much improved in the modified JSBACH, there is a time lag of about 90 days in leaf litter production (See Section 4.1 for discussions).

A comprehensive comparison of the ability of the standard and modified JSBACH to reproduce the observations at TAP is provided in Table 2 (note that the values at the EXP plot are only calculated with data from the first 2 years to exclude the drought-enhanced mortality effects). For LAI, the improvement is apparent at the EXP plot, as the bias, variance and correlation are all much better for the modified JSBACH. Although the improvement is less prominent at the CTR plot (only the bias and CRMSD are better for

the modified JSBACH), we note that it is more important to correctly simulate the drought response at the EXP plot than capturing the non-stressed LAI at the CTR plot within the context of understanding how the Amazon forests respond to future droughts. In addition, although our modification to JSBACH is without drought-enhanced tree mortality, the linear correlation between observation and simulation at EXP plot for all years is still high ( $r = 0.720$ ), indicating that canopy-level leaf shedding is able to explain about half of variance of the LAI reduction due to drought. For leaf litter production, the improvement is prominent at both CTR and EXP plots. Disregarding the lag of about 90 days, the modified JSBACH is able to reproduce the observation at both plots with high correlations, reduced biases and improved seasonal variability.

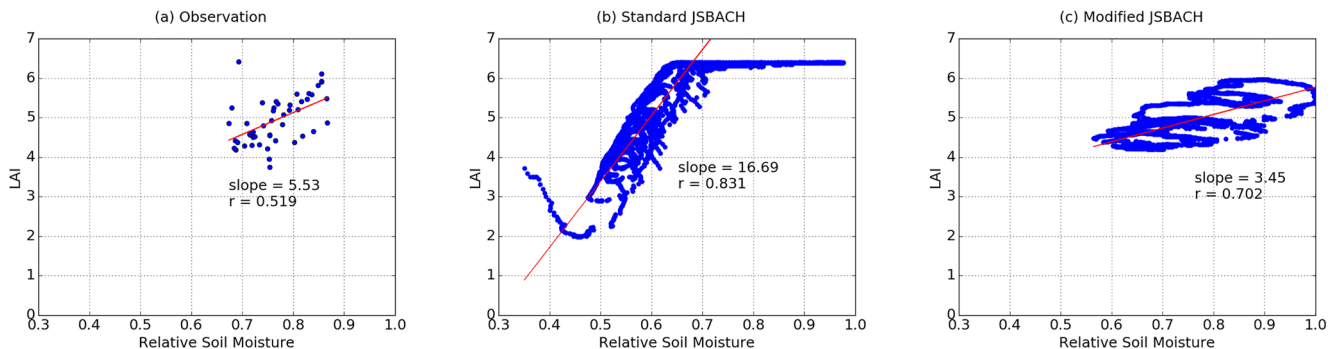


**Figure 3.** Leaf area index (LAI) versus relative soil moisture at the EXP plot (with throughfall exclusion) at Tapajós National Forest of (a) observation, and simulations of (b) standard JSBACH and (c) modified JSBACH. Relative soil moisture is calculated as volumetric soil moisture divided by field capacity. Red lines are regression lines. The regression line in (b) is calculated only when relative soil moisture  $< 0.65$ .

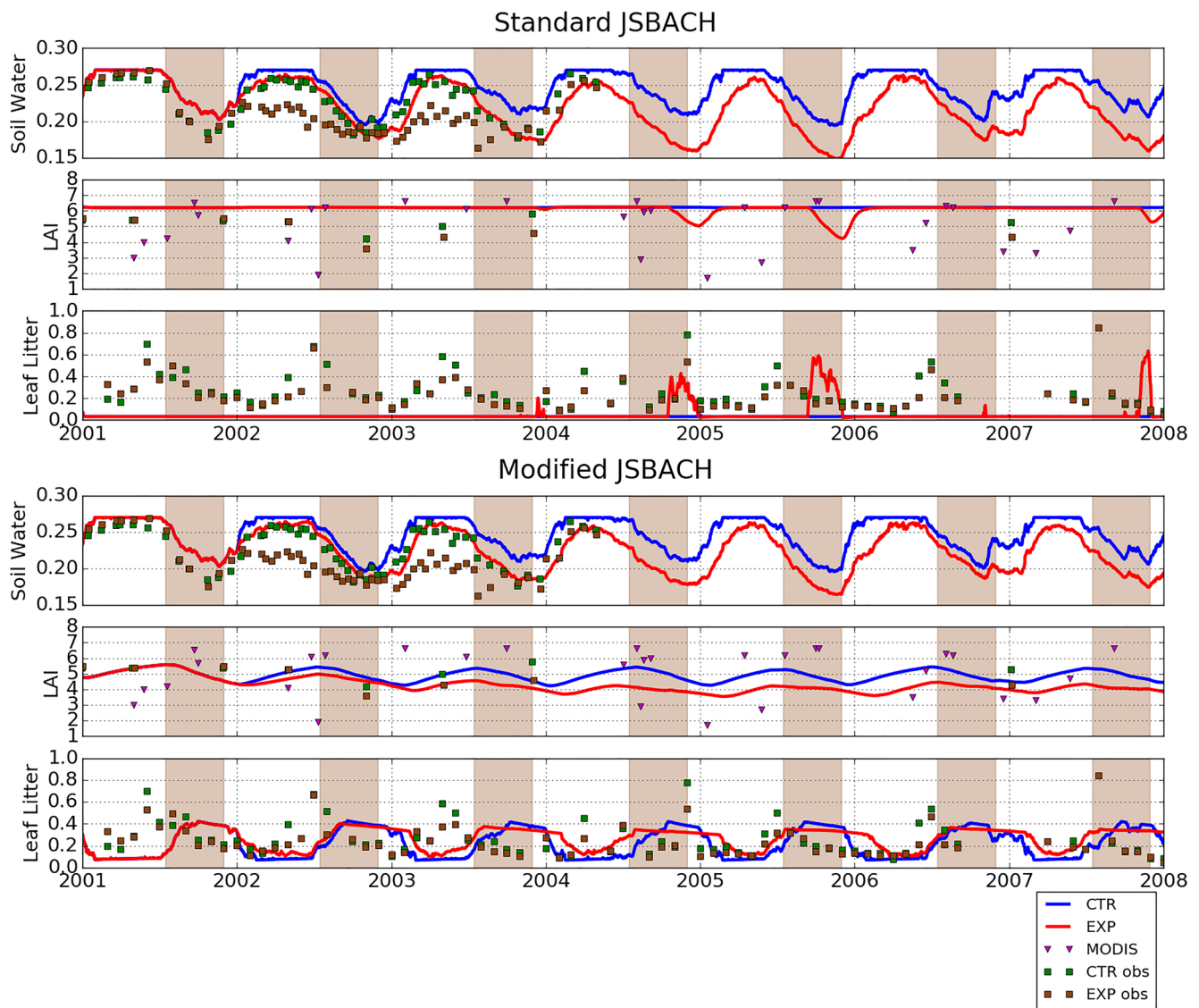


**Figure 4.** Time evolution of soil moisture (top of both panels;  $\text{m}^3/\text{m}^3$ ), LAI (middle of both panels;  $\text{m}^2/\text{m}^2$ ), and leaf litter production (bottom of both panels;  $\text{kg}/\text{m}^2/\text{yr}$ ) of both observations and simulations at the throughfall exclusion experimental site at Caxiuanã National Forest. Two spin-up simulations for reaching equilibrium were conducted for the two model versions respectively, and therefore the initial soil moisture at 2001 is different. (Top) standard (bottom) modified JSBACH. CTR: control plot; EXP: experimental plot (with throughfall exclusion); Dots: in situ observations; Triangles in magenta: MODIS LAI; Lines: simulations. Shading: dry seasons.

The phenology-related parameters in the modified JSBACH are tuned based on the observations at TAP. To test if the modified formulations and parameters are applicable to other sites in the Amazon forests, we carry out the same evaluation at CAX.

The observed and simulated soil moisture, LAI, and leaf litter production at CAX are shown in Figure 4. As shown in the upper row of both panels, the soil moisture at the EXP plot is overestimated by both model versions. A potential reason for the overestimation is the atmospheric forcing data. As described in the simulation protocol in Text S1 in Supporting Information S1, the atmospheric forcing is taken from a global data set at  $0.5^\circ$  resolution, instead of from direct meteorological measurement as in TAP. The forcing is therefore less representative of the situation at the site. For the simulated LAI, similar to TAP, the standard JSBACH simulates mostly constant values of LAI at both CTR and EXP plots (Figure 4, middle row of upper panel). Although measurements were carried out much less frequently at CAX than in TAP, the available observations are already enough to show that LAI is not constant during the experimental period. This is improved in the modified JSBACH (Figure 4, middle row of lower panel), which simulated gentle seasonal variability at both plots.

**Table 3**  
Comparison Between the Standard and Modified Version of JSBACH at Caxiuanã National Forest

Variable	Plot	Version	Bias	dSDev	CRMSD	CCoef
LAI	CTR	Standard <sup>a</sup>	0.987	−0.421	<b>0.436</b>	−0.177
		Modified <sup>a</sup>	<b>−0.404</b>	<b>−0.157</b>	0.537	−0.098
	EXP	Standard <sup>b</sup>	1.324	−0.668	0.681	0.088
		Modified <sup>b</sup>	<b>−0.269</b>	<b>−0.310</b>	<b>0.588</b>	0.508
Leaf litter	CTR	Standard <sup>c</sup>	−0.252	−0.323	0.328	−0.038
		Standard <sup>c,e</sup>	−0.252 <sup>a</sup>	−0.328 <sup>a</sup>	0.328 <sup>a</sup>	−0.141 <sup>a</sup>
		Modified <sup>c</sup>	−0.067	−0.194	0.370	−0.132
		Modified <sup>c,e</sup>	<b>−0.069<sup>a</sup></b>	<b>−0.195<sup>a</sup></b>	<b>0.322<sup>a</sup></b>	<b>0.243<sup>a</sup></b>
	EXP	Standard <sup>d</sup>	−0.287	−0.101	0.113	−0.005
		Standard <sup>d,e</sup>	−0.290 <sup>a</sup>	−0.113 <sup>a</sup>	0.113 <sup>a</sup>	−0.510 <sup>a</sup>
		Modified <sup>d</sup>	−0.108	0.032	0.227	−0.493
		Modified <sup>d,e</sup>	<b>−0.087<sup>a</sup></b>	<b>−0.020<sup>a</sup></b>	<b>0.112<sup>a</sup></b>	<b>0.593<sup>a</sup></b>

Note. At the control plot (CTR), data from all years are used for calculation, while at the experimental plot (with throughfall exclusion; EXP), only data from the first 2 years are used. Values in bold indicate that the respective model version performs better than its counterpart. Values in italic indicate that the correlation is insignificant ( $p > 0.1$ ). Shown are the simulated bias, differences of standard deviation between simulations and observations (dSDev), centered root-mean-square differences (CRMSD), and correlation coefficient with observations (CCoef).

<sup>a</sup> $n = 8$ . <sup>b</sup> $n = 7$ . <sup>c</sup> $n = 96$ . <sup>d</sup> $n = 12$ . <sup>e</sup>Calculated with a lag of 90 days for the simulations.

For the leaf litter production, the results are similar. The standard JSBACH simulates low leaf litter production most of the time at both CTR and EXP plots, with jumps to non-zero values only at the ends of dry seasons at the EXP plot (Figure 4, bottom row of upper panel). In contrast, the modified JSBACH simulates the magnitudes and mean values correctly, despite also having a time lag of about 90 days to the observations (Figure 4, bottom row of lower panel).

A comprehensive comparison of the ability of the standard and modified JSBACH to reproduce the observations at CAX is provided in Table 3. As in TAP, the modified JSBACH is able to reproduce the observed LAI and leaf litter production at both CTR and EXP plots. The evaluation at CAX shows that the improvement by the modified JSBACH at TAP applies also to the simulation at CAX.

To understand whether the improvement of LAI also applies to the whole Amazon, another set of offline experiments are conducted at the scale of the whole Amazon basin (see Text S6 in Supporting Information S1 for details of experimental setup), and the simulated LAI is compared against MODIS data (Figure 5). The LAI from MODIS has a homogeneous spatial pattern over most of NWA, NA, and the northern half of SA (Figure 5a). Compared with the standard JSBACH, the modified version simulates a smaller difference between the mean of NWA and NA, and thus improves in terms of the homogeneity between NWA and NA (Figures 5b and 5c). However, the sharp contrast from high to low LAI over the southern part of SA as seen from MODIS is less evident in the modified JSBACH compared with the standard version. In all three regions, both the standard and modified JSBACH simulate higher LAI compared to MODIS. In addition, the interannual variability of LAI, representing how LAI responds to the interannual fluctuation of soil moisture, is also overestimated by the standard JSBACH. While the ranges of annual mean LAI during 2000–2014 are between 0.2 and 0.3 m<sup>2</sup>/m<sup>2</sup> for

all the three regions in MODIS, the standard JSBACH simulates much larger ranges, from 0.8 to 1.3 m<sup>2</sup>/m<sup>2</sup>. In contrast, the modified JSBACH reduces the overestimated interannual variabilities of the standard JSBACH by 0.4–0.5 m<sup>2</sup>/m<sup>2</sup> at all three regions (Figure S4 in Supporting Information S1). The comparison therefore shows that our modifications to the model are able to improve the simulation of LAI not only at the two TFE sites, but also at different regions of the Amazon basin.

### 3.2. The Direct and LAI Effects of Drought Under Future Climate Simulated by the MPI-ESM

In Section 3.2, we separate the climatic effects caused by drought into the direct effect and the LAI effect with the experimental setup described in Section 2.4. The direct effect refers to the climatic effects caused by soil drying and stomatal responses of plants, whereas such caused solely by the reduction of LAI because of drier soils are referred to as the LAI effect. The total drought effects then indicate the sum of the two effects.

#### 3.2.1. Future Decline of Precipitation and Forcing of the Drought Effects

The spatial pattern of changes in precipitation between the end of the 21st century (2071–2085) and the 20th century (1971–2000) simulated by the MPI-ESM (with the modified JSBACH being the land component) is generally in accordance with the CMIP6 multi-model mean, with prominent reductions in precipitation over central and southern North America, northeastern South America, South Africa, coastal West Africa and Europe (see e.g., Cook et al., 2020). There is also an increase in precipitation in several regions, including central Africa, South Asia, Southeast Asia, and much of the higher latitudes (Figure S5 in Supporting Information S1). Over the Amazon basin, prominent reductions are simulated by the MPI-ESM over northeastern South America (Venezuela, the Guianas, and northern Brazil; Figure 6a). In addition, a stripe pattern exists in parallel with the Andes, such that there are regions of precipitation increase in between the regions of decrease. The stripe pattern is likely

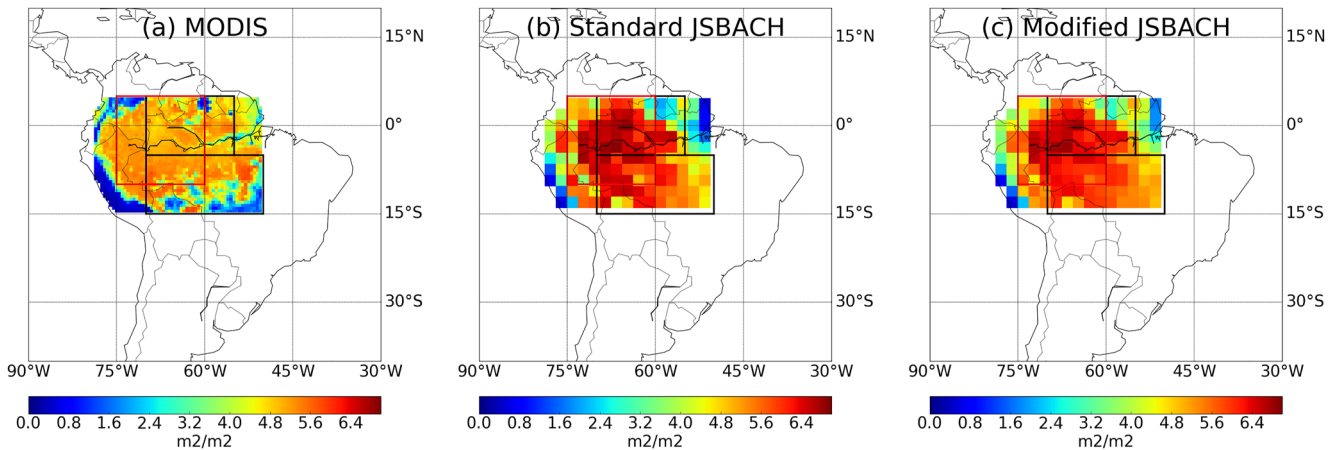


**Figure 5.** Spatial pattern of leaf area index (LAI) from (a) Moderate-Resolution Imaging Spectroradiometer (MODIS) product, simulations of the (b) standard JSBACH, and (c) modified JSBACH, averaged from 2000 to 2014. The black boxes are the Northern Amazon (NA, 70°W–55°W, 5°S–5°N) and Southern Amazon (SA, 70°W–50°W, 15°S–5°S), and the red box is the Northwestern Amazon (NWA, 75°W–60°W, 10°S–5°N), as defined in Yin et al. (2013).

due to the topography, as the Andes are in some regions higher than 4 km in elevation and affect the distribution of water vapor imported from the tropical Atlantic.

Comparing the simulations with the modified and standard JSBACH as the land components, it is found that for the modified JSBACH, the LAI is consistently lower during the historical period (1971–2000) with only small differences in evapotranspiration (ET) and surface temperature over the Amazon (Figure S6 in Supporting Information S1). The forcing of the direct effect for the modified JSBACH during the end of the 21st century is shown in Figure 6b, which is represented by the difference in soil moisture between 21sm–20L and 20sm–20L. Likewise, Figure 6c shows the forcing of the LAI effect, represented by the difference in LAI between 21sm–21L and 21sm–20L. The spatial patterns of the forcing of the direct and LAI effects are similar to the differences in precipitation regarding the negative values, indicating that regions with reduced precipitation experience shortage of soil moisture and reduction in LAI as well (Figures 6a–6c). The connections between precipitation and soil moisture as well as LAI are asymmetric, as the opposite does not hold: regions with increased precipitation do not experience increase in soil moisture. The magnitude of basin-averaged (over the combined Northern and Southern Amazon as shown in Figure 5) changes in precipitation is similar to the magnitudes of the forcing of the direct and LAI effects, which are both about 4%–6% lower relative to their respective 20th-century values. On the other hand, for the standard JSBACH, the forcing of the drought effects under RCP8.5 climate is a similar magnitude of soil drying and a doubled magnitude of the LAI reduction (Figures 6d–6i). The LAI reduction in the standard JSBACH is large because the soil moisture forcing of drought is large enough to exceed the threshold of response, such that the LAI response is more prominent than in the modified JSBACH.

### 3.2.2. Biogeochemical Effects: The Carbon Budget

Figure 7 summarizes the direct and LAI effects on the carbon budget components over the Amazon forests during 2071–2085 of both the standard and modified JSBACH. As the standard JSBACH simulates a strong response of LAI to water stress (Figures 6e and 6f), the LAI effect on GPP reduction is stronger than the direct effect (Figure 7c). Due to the strong reduction in LAI, the decrease in  $R_a$  is also large (Figure 7d) and more than cancels out the reduction in GPP, such that the LAI effect on NPP is between neutral to a weak increase (Figure 7e). The dependence of  $R_a$  on LAI is because  $R_a$  is simulated in JSBACH as the sum of growth respiration ( $R_g$ ) and maintenance respiration ( $R_m$ ), and both  $R_g$  and  $R_m$  are related to LAI.  $R_g$  is associated with NPP, which is higher when LAI is larger, and  $R_m$  is proportional to the dark respiration, which is in turn proportional to LAI (Reick et al., 2021). The direct effect on NPP is negative, as its effect on  $R_a$  is less negative than on GPP (Figure 7e).

For soil respiration ( $R_s$ ), the direct effect is negative, with a magnitude slightly smaller than the decrease in NPP (Figure 7f). The direct effect on  $R_s$  is negative because the soil respiration is sensitive to the limitation of water input and decreases with drier soil, which has also been shown in Meir et al. (2008). In contrast, the LAI effect has an increase on  $R_s$  (Figure 7f). The increase in  $R_s$  due to the LAI effect is because the litter production is increased



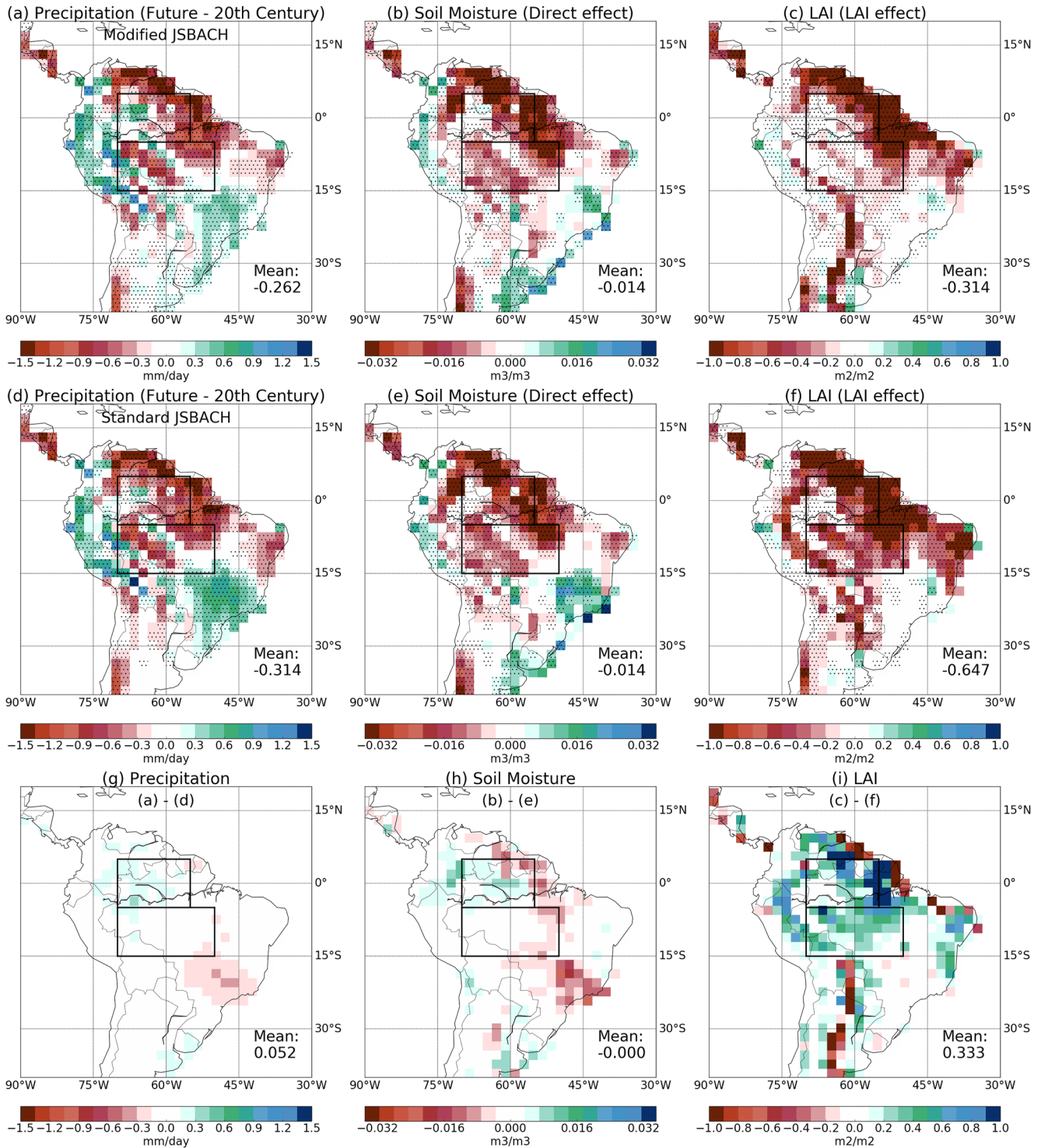


**Figure 6.** (a) Simulated differences of the Max Planck Institute Earth System Model (MPI-ESM, with the modified JSBACH as the land component) in precipitation between the end of the 21st century (2071–2085) and the 20th century (1971–2000). (b) Forcing of the direct effect, represented by the difference in soil moisture between 21sm-20L and 20sm-20L. (c) Forcing of the leaf area index (LAI) effect, represented by the difference in LAI between 21sm-21L and 21sm-20L. (d–f) same as (a–c), but with the standard JSBACH. (g–i) The differences between (a–c) and (d–f). Dots: all ensemble members agree on the signs of change. The mean values are taken over the Northern and Southern Amazon as shown in Figure 5.



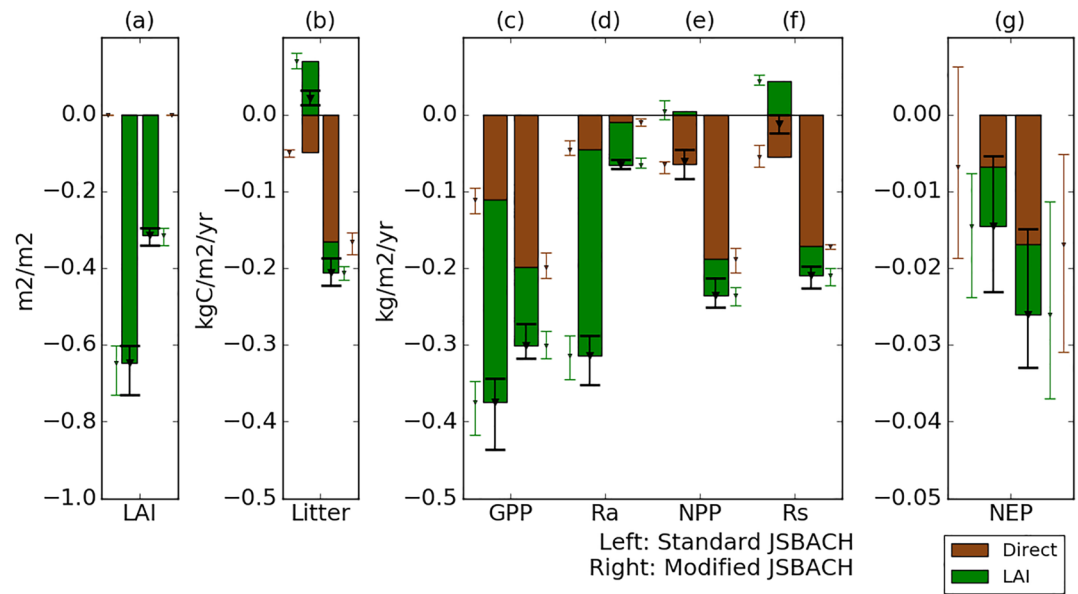


**Figure 7.** The direct and LAI effects of drought on LAI, total litter production, and carbon budget components in the Amazon forests at the end of the 21st century, simulated by the MPI-ESM with the standard and modified JSBACH as the land component. The bars are the differences between experiments as explained in Section 2.4 and represent the magnitudes of the direct and LAI effects averaged over 2071 to 2085. Bars at the left (right) represent the ensemble means of the standard (modified) JSBACH. Whiskers represent the range of ensemble members. GPP: gross primary production;  $R_a$ : autotrophic respiration; NPP: net primary production;  $R_s$ : soil respiration; NEP: net ecosystem production. The values are averaged over the regions of the Northern and Southern Amazon as shown in Figure 5.

(Figure 7b). For the standard JSBACH, the leaf litter production depends on the net change in LAI when LAI is decreasing faster than the pre-defined aging rate (Equation 9). As the LAI in 21sm-21L experiences more soil water stress compared with in 21sm-20L, the long-term averaged negative change in LAI and in turn the litter production is larger in 21sm-21L. The LAI effect on litter production and  $R_s$  is therefore positive and reflects the change in LAI seasonality under future climate simulated by the standard JSBACH. For both the direct and LAI effects, the net effects on net ecosystem production (NEP) are negative (Figure 7g). While both the direct and LAI effects are subject to large internal variability, for the direct effect the range of uncertainty is larger, as the change in NEP can be positive in specific ensemble members.

For the modified JSBACH, the reduction in GPP due to the direct effect is stronger than the LAI effect, which is opposite to the results of the standard JSBACH (Figure 7c). The reduction in GPP is also stronger than in the standard JSBACH, which could be related to several factors. For example, while the reduction in soil moisture and LAI of the two versions are similar, their biogeophysical effects are different (Section 3.2.3). The enhancement of surface net shortwave radiation and surface temperature are both stronger for the modified JSBACH. As GPP is also affected by biogeophysical terms including radiation and temperature, the simulated reduction in GPP can be different between the standard and modified JSBACH. Compared to the GPP reduction, the direct effect on  $R_a$  is much weaker and close to neutral (Figure 7d). In contrast, the LAI effect on  $R_a$  is stronger and compensates about half of the reduction of LAI effect on GPP. Due to strong reduction in GPP and weak reduction in  $R_a$ , the direct effect on NPP reduction is strong (Figure 7e). For the LAI effect, as the reduction in GPP is weak and the reduction in  $R_a$  is strong, the net effect on NPP is weak negative, which is opposite from the neutral to positive sign simulated by the standard JSBACH. Aside from the different signs of change of the LAI effect on NPP, the reduction in NPP from the direct effect is also stronger than in the standard JSBACH.

For both the direct and LAI effects, the reduction in  $R_s$  is slightly less than the reduction in NPP, which is another major difference between the standard and modified JSBACH (Figure 7f). While the standard JSBACH simulates an increase in  $R_s$  from the LAI effect, a decrease is simulated by the modified JSBACH. As in the standard JSBACH, the LAI effect on  $R_s$  is related to the change in litter production. As shown in Figure 7b, the LAI effect on total litter production is a decrease for the modified JSBACH, while for the standard JSBACH it is an increase.

For the modified JSBACH, the leaf litter production depends on the shedding rate and LAI itself (Equation 10). When calculating the LAI effect, since the soil moisture in 21sm-21L and 21sm-20L are the same, the shedding rate is the same. Therefore, because the LAI in 21sm-21L is lower than in 21sm-20L, the LAI effect on litter production is negative, which reflects the fact that less litter can be produced from lower LAI under future drought condition. A large part of the NPP reduction is therefore canceled out by the reduction in  $R_s$ . The NEP is negative for both the direct and LAI effects, and the magnitudes are larger than the standard JSBACH (Figure 7g). In contrast to the standard JSBACH, the LAI effect is more subject to the uncertainty associated with internal variability. The direct effect on NEP is about twice the magnitude as the LAI effect, and thus, the LAI effect accounts for about 35% of the total drought effects ( $9 \pm 10$  vs.  $26 \pm 7$  g/m<sup>2</sup>/yr; mean  $\pm$  1 sd). Compared with the NEP between 1971 and 2000, the NEP reduction due to direct and LAI effects corresponds to reduction of 25.4% and 13.8% respectively, which are larger than the magnitudes of the forcing (about 4%–6%).

In the responses of the carbon budget components to the drought effects, the ensemble members generally agree well with each other over most parts of the Amazon in the signs of change (Figures 8a and 8b and Figure S7 in Supporting Information S1, including the weak responses of  $R_a$  and  $R_s$ ). However, NEP is an exception. For NEP, while the mean effects over the whole Amazon are prominent (Figure 7), for many of the grid points, the ensemble members do not agree with each other on the sign of change (Figures 8c and 8d). This is because NEP is the net flux of the larger gross fluxes of NPP and  $R_s$ , and as the magnitudes of reduction in NPP and  $R_s$  are similar, it is sensitive to noises such that in large parts of the NA and almost the whole SA, whether the effect is positive or negative, is subject to the internal variability.

### 3.2.3. Biogeophysical Effects: The Surface Energy and Water Budgets

Figure 9 summarizes the drought effects on the biogeophysical terms in the Amazon forests during 2071–2085 of both the standard and modified JSBACH. For the standard JSBACH, the direct effect contributes to a reduction in soil evaporation, while the LAI effect is an increase (Figure 9a). The reason is that more radiation is able to reach the surface to evaporate soil moisture due to the prominent reduction in LAI. For the same reason, the LAI effect on reduction in transpiration is also large, and larger than the contribution from the direct effect (Figure 9b). The reduction in latent heat flux results in a reduction in low cloud cover, as well as an increase in net surface short-wave radiation (Figures 9c–9e). Through the land-atmosphere interaction, the result of the combined drought effects is an increase in surface temperature of about 0.7 K (Figure 9f).

For the modified JSBACH, the direct effect reduces both soil evaporation and transpiration strongly (Figures 9a and 9b). In contrast, the LAI effect is close to zero on soil evaporation, and the reduction in transpiration is much less than the direct effect. For the direct effect, the reduction in transpiration is 30% higher than in soil evaporation, indicating that the contribution from stomatal response is larger than soil response. Despite the different signs of change and magnitudes of the LAI effect on soil evaporation and transpiration compared with the standard JSBACH, the sum of the direct and LAI effects on latent heat flux does not differ much from the standard JSBACH (Figure 9c). As in the results of standard JSBACH, a reduction of more than 1% of low cloud cover as well as an enhancement in net surface solar radiation of more than 1.5 W/m<sup>2</sup> is found (Figures 9d and 9e). Similar to the standard JSBACH, the combined drought effects on the surface temperature is a warming of about 0.7 K, with the direct effect being stronger than the LAI effect by a factor of 7 (Figure 9f). The LAI effect thus accounts for about 12% of total drought-induced surface warming ( $0.09 \pm 0.03$  vs.  $0.7 \pm 0.07$  K).

While the surface warming due to both the direct and LAI effects are homogeneous in sign and similar in strength across the Amazon (Figures 10a and 10b), the effects on precipitation have a dipole pattern (Figures 9g and 9h). The direct effect results in an increase of precipitation over the NA, and a decrease over the SA (Figure 10c). The south-north cross-section in Figure 10e shows the distribution of wind and moisture in wet (20sm-20L) and dry minus wet (21sm-20L minus 20sm-20L) experiments. The drying over the NA and the associated heating creates anomalous upward motion in locations where the original moisture is already abundant, which favors moist convection and hence enhances the precipitation there. On the other hand, reduced convection is found over the SA, leading to reduction in precipitation. While the direct effect on precipitation change is prominent, the contribution from the LAI effect is negligible (Figures 9g, 9h, and 10d). For the direct effect, the evaporative demand from the atmosphere (represented by the potential evapotranspiration, PET) is increased in both the Northern and SA (Figures 9i and 9j). With the changes in precipitation and PET, we calculate the change in aridity, represented

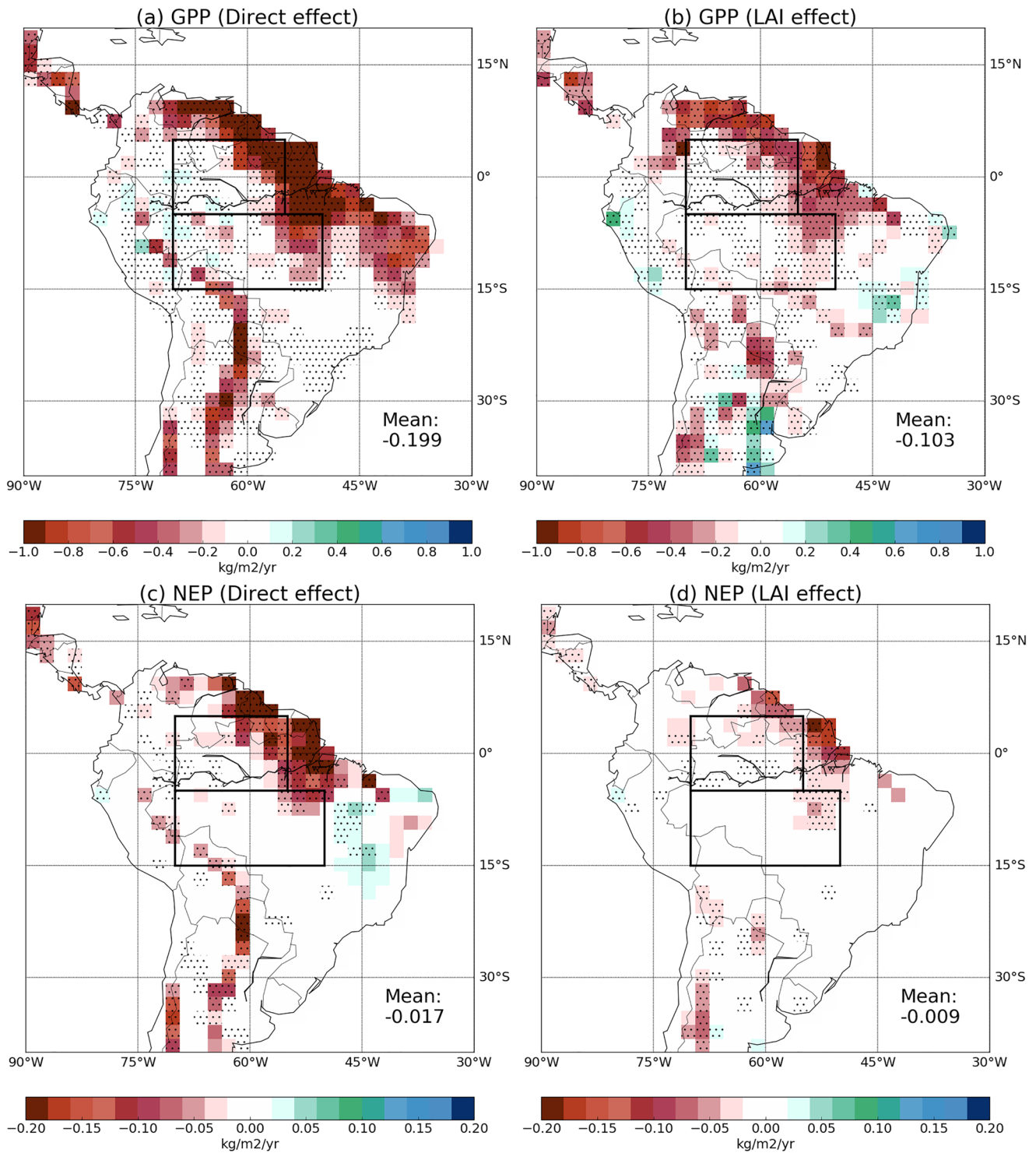


**Figure 8.** Spatial pattern of the direct and LAI effects on different carbon budget terms during 2071–2085. GPP: gross primary production; Ra: autotrophic respiration; NPP: net primary production; Rs: soil respiration; NEP: net ecosystem production; Dots: All ensemble members agree on the signs of change. The mean values are taken over the Northern and Southern Amazon as shown in Figure 5.

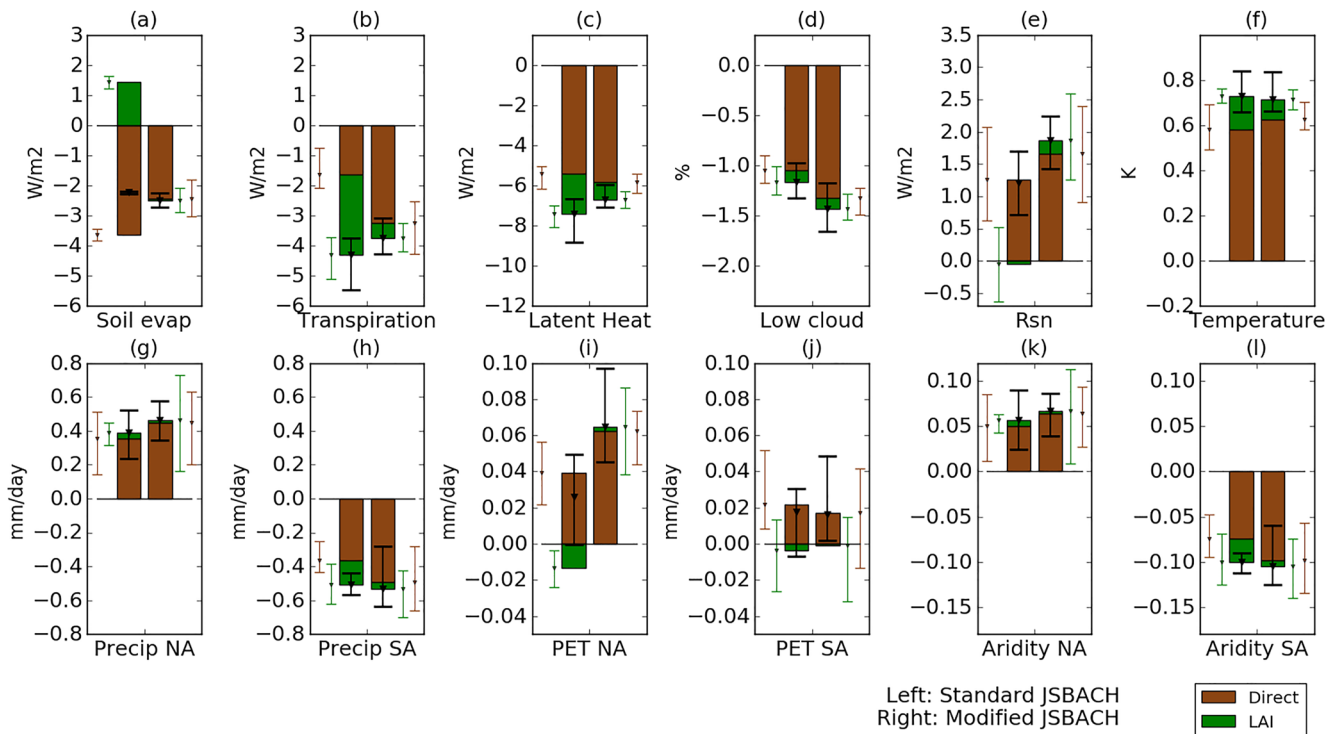


**Figure 9.** The direct and leaf area index (LAI) effects of drought on biogeophysical terms in the Amazon forests at the end of the 21st century, simulated by the Max Planck Institute Earth System Model (MPI-ESM) with the standard and modified JSBACH as the land component. The bars are the differences between experiments as explained in Section 2.4 and represent the magnitudes of the direct and LAI effects averaged over 2071 to 2085. Bars at the left (right) represent the ensemble means of the standard (modified) JSBACH. Whiskers represent the range of ensemble members. Soil evap: soil evaporation; Rsn: net surface shortwave radiation; Precip: precipitation; PET: potential evapotranspiration calculated with the Priestley-Taylor equation (Priestley & Taylor, 1972); Aridity: aridity Index, calculated as the ratio between precipitation and PET. The values of the upper row are averaged over the regions of the Northern (NA) and Southern Amazon (SA) as shown in Figure 5. The values of the lower row are averaged over NA and SA, respectively.

as the Aridity Index (AI, the ratio between precipitation and PET; Figures 9k and 9l). Note that higher AI indicates less dryness. Despite the predominantly soil drying pattern across the Amazon (Figure 6b), the signs of change of aridity are different in the NA and SA. The aridity is reduced in the NA (an increase in AI), while in the SA the aridity is increased (a decrease in AI). Therefore, in both the Northern and SA, the change in aridity is decided by the changes in precipitation, while the increased PET plays a minor role. Finally, we note that for the precipitation, PET and AI, the standard and modified JSBACH predict similar results at both the Northern and Southern Amazon.

## 4. Discussion

### 4.1. Site-Level Evaluation: Implications for Future Model Development

Previous studies have shown that current state-of-the-art models are unable to reproduce the responses to drought in the TFE experiments including LAI and carbon fluxes (Joetzjer et al., 2014; Powell et al., 2013). Our evaluation shows that this is also the case for the standard JSBACH. Several implications are drawn for future model development. We note that as we focus on the time scales of episodic to multiyear drought and utilize the data from TFE experiments, the results have less implication for seasonal drought in semi-deciduous forests (see e.g., Vourlitis et al., 2008).

A simulated constant LAI or lack of seasonality simulated by the standard JSBACH as well as mismatches between simulations and observations have also been found in other models (Restrepo-Coupe et al., 2017), and a constant leaf shedding rate is assumed for evergreen trees in several models within the CRESCENDO project, which contains a total of seven ESM groups (Peano et al., 2020). The constant LAI is aimed to simulate the

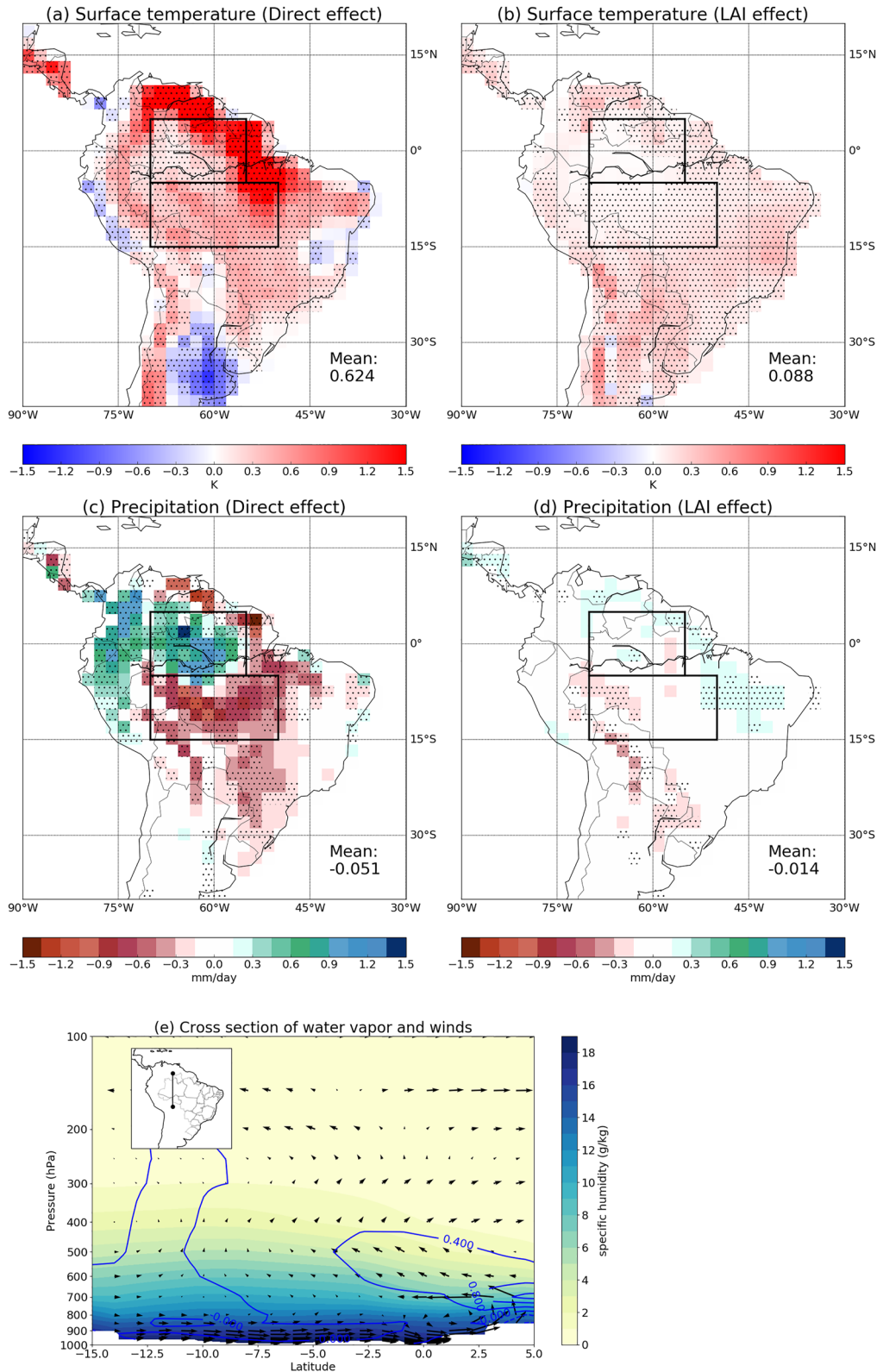


**Figure 10.** (a) Change in surface temperature due to the direct effect. (b) Change in surface temperature due to the LAI effect. (c) Change in precipitation due to the direct effect. (d) Change in precipitation due to the LAI effect. (e) North-south cross-section of wind and moisture field between wet (20sm-20L) and dry (21sm-20L) experiments during late 21st century. Vector: (meridional wind, pressure velocity ( $-10 \times \omega$ )); contour: change in specific humidity; shading: specific humidity in the wet experiment. From (a) to (e): during late 21st century (2071–2085).



low LAI seasonality of tropical evergreen trees compared to deciduous trees. While a constant LAI for tropical evergreen trees might be intuitive, whether vegetation indices of tropical evergreen trees have seasonal variability has sparked discussion. It has been shown in a satellite-based study that the canopy is not constant throughout the year, with a swing of about 25% in green leaf area observed in a majority of the Amazon forests (Myneni et al., 2007). At TAP, the observed LAI at the CTR plot has an annual range of larger than  $2 \text{ m}^2/\text{m}^2$ , which is more than 30% of the mean value (Figure 2). Several factors have been proposed to contribute to the seasonality of vegetation indices of the Amazon forests, such as the seasonal variation in available solar radiation and soil moisture (see e.g., Baker et al., 2009; Bradley et al., 2011; Kim et al., 2012). It has been shown that seasonal variability of GPP is associated with leaf phenology, which can be linked to soil moisture as the seasonal water stress in the Amazon forests is synchronized with leaf flushing and in turn affects the photosynthesis (Brando et al., 2010). As water stress has been shown to have a first-order control on vegetation seasonality in global tropical forests (Guan et al., 2015), and leaf shedding has been suggested as a strategy of plants for drought avoidance (Munné-Bosch & Alegre, 2004; Polle et al., 2019), it is crucial for models to simulate the LAI variation within annual scale.

In this study, we modified JSBACH to improve the canopy dynamics. The fact that the improvement at TAP is transferable to another independent TFE experimental site at CAX (Table 3) and different regions of the Amazon basin (Figure 5) indicates the tuning utilized in this study is applicable in the Amazon forests.

In the TFE experiments, an enhanced tree mortality is observed after roughly two years of experiments, which results in larger decline in LAI (Brando et al., 2008; Meir et al., 2015). Similarly, a strong reduction in LAI following severe drought is also observed from the natural droughts, which can be associated with enhanced tree mortality (e.g., Lewis et al., 2011; Phillips et al., 2009). To account for the enhanced mortality but still maintain a stable LAI within annual time scale, the standard JSBACH assumes a soil moisture threshold only below which LAI starts to reduce, and adds a strong dependence of LAI to soil water content. However, in reality, mortality occurs at the individual scale and leaf shedding is at the leaf scale. Therefore, the two effects should not be mixed together and the lack of mortality should not be compensated with an unrealistically strong leaf shedding. This is similar to what was pointed out in Rowland et al. (2015), where the inconsistency across models simulated at leaf level is masked by the inconsistently simulated LAI response. While the stand-level drought response of enhanced mortality is not yet included in the model, by enabling JSBACH to simulate correctly the mild LAI reduction within annual time scale and under mild drought, we can constraint the canopy-level responses of the Amazon forests to future droughts. The uncertainty of the overall responses to future droughts will thus be reduced when the enhanced tree mortality is included in the model. It is noteworthy that the linear correlation of the simulated and observed LAI at TAP during the whole experimental period is not vastly lower than the first two years, indicating that the modified JSBACH is already able to reproduce large portion of the LAI variability despite lacking a representation of the enhanced mortality.

Similar to LAI, current vegetation models simulated litter flux with a large spread and are not able to reproduce the results at the TFE experimental sites well (Powell et al., 2013). The standard JSBACH is not an exception and simulates the litter flux at both TAP and CAX with negative biases. The annual-mean biases and variance are largely improved in the modified JSBACH, although the parameters are tuned against observed LAI instead of observed leaf litter flux, which indicates the fidelity of the modified formulation as well as the importance for future model development to couple leaf litter production with leaf phenology. However, the seasonality is simulated with a lag of roughly 90 days. There are several candidates for the reason of the 90-day lag. While we assume the leaf shedding rate to depend solely on soil moisture, water stress is perceived by plants as an insufficient soil water supply to fulfill the atmospheric demand driven by vapor pressure deficit and therefore involves both land and atmosphere conditions, which might have a difference in time. Previous studies have also indicated that leaf demography (e.g., explicit representation of leaf ages, which is currently not represented in JSBACH) and the synchronization of leaf flushing and leaf litter production play important roles in simulating carbon flux seasonality in the Amazon forests (Doughty & Goulden, 2008; Lopes et al., 2016; Manoli et al., 2018; Wu et al., 2016). Meanwhile, leaf quality has been shown to play an important role in the leaf response to seasonal drought (e.g., Wu et al., 2018; Wu, Guan, et al., 2017), and might help improve the seasonality of leaf litter production. However, for the purpose of this study, which is to separate the direct and LAI effects to episodic and multiyear droughts, the focus is thus placed on leaf quantity (LAI). As leaf demography has less impact on water and energy fluxes (Manoli et al., 2018), and we are currently interested in the impacts of droughts on mean-state

climate, which relates more to the annual mean value than the seasonality of leaf litter, we leave the issue of improving leaf litter seasonality for future exploration.

#### 4.2. Quantifying the LAI Effect of Droughts Under Future Climate

In this study, the drought effects on climate are separated into (a) the direct effect, which results from both drier soil and the physiological response of stomatal closure, and (b) the LAI effect, which results from changes in LAI and in turn results from the drier soil (Figure 1). Therefore, the LAI effect contains the effects due to perturbations in canopy structure, while the direct effect is associated with the soil and physiological effects and unrelated to changes in LAI. The importance of the LAI on GPP in the Amazon forests has been investigated in Flack-Prain et al. (2019), where the LAI is included as an important component of the so-called indirect effect of drought. It was found that the variation of LAI is more important than the direct effect in determining the spatial pattern in GPP across the drought stress gradient in the Amazon forests. On the contrary, at seasonal time scale, the direct effect was shown to be more important than the indirect effect. Our findings are able to complement the results from Flack-Prain et al. (2019). Flack-Prain et al. (2019) argued that a shift from direct to indirect pathways exists when time scales are longer. Our results show that for the interannual time scale of episodic to multiyear droughts, the LAI effect does not dominate over the direct effect as in determining the spatial pattern. However, the LAI effect is still important and not negligible. The interannual time scale is therefore a transitional regime between the direct- and indirect-dominating time scales that both the direct and LAI effects are important and should be taken into account.

Due to the importance of LAI in determining terrestrial carbon budget in the Amazon forests, it is crucial to quantify the contribution of the LAI effect under future climate. However, in previous studies on future drought effects such as the GLACE-CMIP5 experiment, the drought effects were often implicitly perceived as solely from the drier soil, and even as the responses from leaf dynamics are included, the relative importance of the direct effects compared to the subsequent leaf shedding was not quantified. With the improved ability of the modified JSBACH to simulate LAI response to drought, our results thus provide better insights into the role of the LAI effect under future climate.

Our results show that for the terrestrial carbon budget terms, the contribution of the LAI effect is large. The reduction in land carbon uptake (NEP) during 2071–2085 due to the LAI effect accounts for 35% of the total drought effects. As the total drought effects induce 40% of NEP reduction compared with the 1971–2000 value, the LAI effect alone is able to reduce about 14% of the natural carbon uptake in the Amazon. We note that both the direct and LAI effects on NEP are amplifying the original drought forcing. The decline in NEP due to the direct effect (LAI effect) is 25.4% (13.8%), compared to the original forcing of the decline in soil moisture and LAI, which is only ca. 4%–6% (Figure 6).

While Flack-Prain et al. (2019) focused on the comparison between the direct and indirect effects on GPP under current climate and Green et al. (2019) discussed only the drought effects on NEP, in this study, we focus on future climate and extend the analysis to the terrestrial carbon budget terms. The NEP can be decomposed into GPP, autotrophic production ( $R_a$ ), soil respiration ( $R_s$ ), and the difference between GPP and  $R_a$  is NPP. Across these carbon budget terms, the ratios of the magnitude of the direct to LAI effects are different, ranging from 0.2 for  $R_a$ , to 4.4 for  $R_s$ , which reflects that the LAI effect plays different roles for different carbon budget terms. Therefore, directly looking into NEP may lead to omission of important insights, as different carbon budget terms are regulated by different mechanisms and models might give the right results for wrong reasons. Studies on the mechanisms of all the underlying variables including below ground vegetation responses are thus necessary for further process understanding.

To illustrate the importance and complexity of looking into different carbon budget terms, we note, for example, that NPP is affected by the limitation of soil water and at the same time impacts ecosystem functioning and leaf litterfall. In JSBACH, NPP also depends on soil water via several pathways. NPP is calculated in JSBACH as the difference between GPP and  $R_a$ . The GPP is calculated as the multiplication of LAI and carbon assimilation per leaf area, and the carbon assimilation is limited by soil water stress via a water stress function (Section 2.3.1).  $R_a$  can be separated into the growth respiration ( $R_g$ ) and maintenance respiration ( $R_m$ ). As mentioned in Section 3.2.2, both  $R_m$  and  $R_g$  depend on LAI and are affected by NPP. Therefore, via the abovementioned pathways, JSBACH

considers both directly and indirectly the effects of soil moisture limitation and at the same time feedback to ecosystem functioning and LAI.

For the biogeophysical effects, both the direct and LAI effects contribute to surface warming, implying that through the land-atmosphere interactions, the drought effects act to enhance the surface warming under climate change, which is in line with the results globally as calculated in the GLACE-CMIP5 experiment (Berg et al., 2016). The magnitude of surface warming due to the combined drought effects ( $\sim 0.7$  K) is close to the magnitude of the warming-induced in a total-deforestation scenario of the Amazon forests (Lejeune et al., 2015), which is not trivial. Our results further show that the contribution of the LAI effect on surface warming is 12% of the total drought effects, which is smaller compared to the contribution of the LAI effect on NEP (35%). Compared to the biogeochemical effects, the LAI effect usually plays smaller roles in terms of biogeophysical effects. While LAI is able to affect atmospheric boundary layer via modifying the albedo and surface roughness, the LAI effect on the precipitation, potential evapotranspiration (PET) and aridity is negligible compared to the direct effect. To sum up, the LAI effect is a significant component of drought impacts for at least the carbon and surface energy budget via the biogeochemical and biogeophysical effects, and should be carefully considered in the land surface models within the ESMs in order to have more precise future projection on future climate.

#### 4.3. Comparison Between Model Uncertainty and Internal Variability

The long-term land carbon uptake has been predicted by the ESMs with large uncertainties. The uncertainty in land carbon uptake across the CMIP5 models was shown to be comparable with the spread due to different scenarios (Jones et al., 2013). Several components contribute to the large uncertainties. In a coupled climate system, the internal variability arises from the intrinsic chaotic behavior of the system and causes uncertainty in the climate. Tokarska et al. (2020) showed that internal variability contributes approximately  $\pm 0.09$  K to the uncertainty of anthropogenic warming to-date, corresponding to a remaining carbon budget of  $\pm 30$  to  $\pm 50$  PgC, which is up to 46% of the remaining budget for 1.5 K. On the other hand, the model uncertainties, which root from the different process parameterizations and parameter values utilized in the models, also contribute to the uncertainties in model simulations. For example, Raczka et al. (2018) showed from the simulations at Northern Wisconsin that the leaf-level parameters contribute the most uncertainty for long-term projections of NEP, NPP and aboveground biomass and the fast physiological responses contributes the most to land carbon uptake regardless of time scale. Understanding the sources of uncertainties help reduce the uncertainties and will in turn enhance the ability of models predicting future climate. In this study, the experimental setup enables the quantification of the model uncertainty in carbon cycle associated with the different formulations of LAI and leaf litter production (the standard vs. modified JSBACH) as well as the uncertainty arising from the internal variability (given by the spread of results among the five ensemble members). As the focus of this study is on the LAI, which is relevant to the exchange of carbon, water and momentum between the land and the atmosphere, the comparisons on different uncertainties are extended from the biogeochemical effects to also the biogeophysical effects.

For the carbon budget terms, our results show that the model uncertainty is large, as several terms are simulated quite differently between the standard and modified JSBACH, and some of them have different signs of change (Figure 7). In a recent study utilizing the GLACE-CMIP5 experiment, it was found that variability in soil moisture contribute 90% of interannual variability in global land carbon uptake, and most of the influences are indirect responses via the soil moisture-atmosphere feedback instead of direct responses from the soil moisture (Humphrey et al., 2021). Our results further separate the uncertainties of the direct and LAI effects. The signs of change in NPP and  $R_s$  from the LAI effect are different between the standard and modified JSBACH, which is caused solely by modifying the LAI and leaf litter formulation, indicating that having a better LAI response to water stress can be equally important as having better formulations of the photosynthesis and respiration fluxes themselves. In comparison, the uncertainty associated with internal variability is generally smaller and the signs of change due to the drought effects are consistent across the whole Amazon basin. In fact, the simulated differences in NEP in the Amazon basin between the end of the 21st (2071–2085) and 20th century (1971–2000) by the two model versions are differed by 15%, which is larger than the spread caused by the internal variability (10% and 11%). Our results can be compared with previous studies, which showed with a series of LSM simulations that the climate uncertainty due to different forcing (which can represent internal variability in uncoupled configuration) exceeds the model uncertainty in historical periods (Bonan et al., 2019), and that the internal

variability plays an important role in determining the NEP in North America such that ensemble mean should be considered instead of any single ensemble member (Bonan et al., 2021). Several factors likely contribute to the different results between this study and previous studies. While Bonan et al. (2019) utilized different versions of the Community Land Model, JSBACH is utilized in this study. Although different climate forcing is viewed to represent internal variability, the mechanism is intrinsically different from ensemble simulations, and it is likely that the uncertainties produced by different climate forcing are different from produced by ensemble simulations. Finally, in Bonan et al. (2021) where the ensemble simulations were utilized, they focus on North America, which is a different climate zone than the Amazon, which might also be a reason why their results are different from this study.

For the biogeophysical effects, although the LAI effect is in general less important in the modified JSBACH than in the standard JSBACH, the differences between the two model versions are smaller, and the results are qualitative similar compared to the carbon budget terms (Figure 9). The LAI is expected to affect biogeophysical effects in several aspects, but while the model uncertainties of soil evaporation and transpiration are large, the model uncertainty of the latent heat flux is smaller. When compared between the end of the 21st and 20th century, the model uncertainty of latent heat flux is much less than the spread among ensemble members for the both model versions (60% of model uncertainty compared with 420% and 98% of spread among ensemble members due to internal variability). The smaller model uncertainty than internal variability also applies to the increase of surface temperature, with only 0.33% of model uncertainty compared with 2.1% and 6.4% of spread among ensemble members.

#### 4.4. Drought Amplification Due To the Direct Effect

While the spatial patterns of drought effects on carbon budget terms are similar to the drought forcing and are homogeneous across the Amazon basin (Figure 6), a non-local pattern of north-south dipole exists for the change in precipitation (Figure 10). The reduction in precipitation over southeastern Amazon due to the direct effect indicates that over the southeastern Amazon, the direct effect is able to form a positive feedback and amplify the original drying forcing. Previous studies have also investigated the feedback between drought and vegetation responses in the Amazon basin in different contexts, such as forest loss and deforestation. A positive feedback has been found between drought and land cover change in the SA near the arc of deforestation (Bagley et al., 2014) or southwestern Amazon (Staal et al., 2020), as the land cover change from rainforest to pasture or cropland in the Amazon region is able to reduce precipitation and increase the magnitude of droughts. Similarly, in Zemp et al. (2017), a positive feedback between reduction in dry-season rainfall and forest loss was found in the Amazon basin. The forest loss was shown to amplify itself as the resultant reduction in evapotranspiration (ET) favors the conversion from high tree cover to low tree cover, which mostly takes place in southeastern Amazon.

While the amplified drying over the SA is consistent with previous studies (Bagley et al., 2014; Staal et al., 2020; Zemp et al., 2017), we note that the amplified drying is induced by the direct effect, indicating that an amplification of drying does not necessarily require changes in canopy structure, enhanced mortality, or land cover change. Moreover, our results also show an increase in precipitation over the NA, which was not apparent in previous studies. A meridional dipole of increase in the north and decrease in the south indicates a redistribution of precipitation and is dominated by dynamical feedbacks. While an increase in precipitation due to soil drying in the tropical rainforests may be counterintuitive, it has been found in previous studies investigating the effects of deforestation in the Amazon basin (Boysen et al., 2020; Lejeune et al., 2015) and the Maritime Continent (Chen et al., 2019). On the other hand, reduced precipitation over wetter soil in the Amazon forests has also been simulated in previous studies with different models (Harper et al., 2014; Lin et al., 2015), indicating that local ET is not the sole factor determining precipitation in this region and dynamical mechanisms are important in determining precipitation response.

In the GLACE-CMIP5 experiment, the global mean aridity was shown to enhance due to soil drying under global warming (Berg et al., 2016). However, it was not clear whether the enhanced aridity is consistent across the globe. In our results, a consistent enhanced aridity due to drought is not found over the whole Amazon forests. Instead, the aridity change due to drought follows the pattern of precipitation change. The aridity is reduced in the NA and an enhancement is found in the SA. Since the SA may be subject to a tipping point of drastic vegetation shift (e.g., Fearnside, 2018; Nobre et al., 2016), an amplified rainfall reduction and aridity enhancement over the SA

may further endanger the vegetation there under future climate. We suggest that future studies should focus on quantifying the remaining carbon budget for a tipping point in the Amazon forests.

## 5. Summary and Conclusions

The Amazon forests are the largest rainforests and living carbon reservoirs of the terrestrial ecosystem, and play important roles in regional climate. However, the Amazon region is predicted to experience more droughts in the future with a decreased mean state of precipitation and increased seasonal variability. Previous studies have shown that current vegetation models are poor in capturing vegetation drought responses in the Amazon forests. Biases therefore exist in the simulated future climate and carbon budget by ESMs, and it is crucial to quantify the model uncertainty related to vegetation drought responses. In this study, a series of experiments have been conducted with the land surface model JSBACH and insights into the drought effects have been provided for the modeling community.

We investigate the ability of JSBACH to capture vegetation drought responses, characterized by the drought impacts on LAI and leaf litter production, with observations from the two TFE experimental sites in the eastern Amazon forests. The evaluation shows that the standard JSBACH fails to reproduce the LAI and litter production as observed in the TFE experimental sites. Modifications are implemented to the formulations of LAI and leaf litter production. Several implications for future model development are highlighted. First, the LAI growth should be coupled with the plant production in order to simulate the seasonality of LAI and correctly incorporate the interaction between climate and vegetation growth. In addition, drought responses of different scales should be modeled at the respective scales. Finally, the results show that tuning model against the intensive data from field campaigns is promising.

With the modified JSBACH as the land component, coupled land-atmosphere simulations are conducted to separate the direct and LAI drought effects. The direct effect refers to the drought impacts directly resulting from drier soil and stomatal response and does not involve change in LAI, whereas the LAI effect refers to the drought impacts resulting from leaf shedding (lower LAI), which is in turn due to drier soil. It is shown that the LAI effect is important for both the carbon and surface energy budget terms, with a stronger effect on the former. The contribution of the LAI effect relative to the total drought effects during 2071–2085 is 35% in reducing land carbon uptake, and 12% in increasing the surface temperature. We also compare (a) the model uncertainty associated with the formulations of LAI and leaf litter production, and (b) the uncertainty due to the internal variability. For carbon budget terms, the former is larger, while for latent heat flux and surface temperature, the latter is much more important. Large uncertainties and biases therefore exist in the predictions of future carbon budgets by current vegetation models. To address the question, better strategies in modeling leaf phenology including more mechanically based or observation-based approaches as implemented in this study should be adopted.

## Data Availability Statement

The model codes, scripts, and information on how to repeat the simulations and analysis presented in this study are archived at the publication repository of the Max Planck Society (<http://hdl.handle.net/21.11116/0000-0009-7975-C>).

## Acknowledgments

This research was supported by the German Research Foundation (DFG; grant no. PO1751/1-1). All simulations have been conducted at the German Climate Computing Center (DKRZ; allocation bm0891). The authors would like to thank Andreas Chlond for helpful comments. The authors also thank the reviewers for their constructive comments that helped to improve the quality of the manuscript. Open access funding enabled and organized by Projekt DEAL.

## References

- Bagley, J. E., Desai, A. R., Harding, K. J., Snyder, P. K., & Foley, J. A. (2014). Drought and deforestation: Has land cover change influenced recent precipitation extremes in the Amazon? *Journal of Climate*, 27(1), 345–361. <https://doi.org/10.1175/JCLI-D-12-00369.1>
- Baker, I. T., Prihodko, L., Denning, A. S., Goulden, M., Miller, S., & Da Rocha, H. R. (2009). Seasonal drought stress in the Amazon: Reconciling models and observations. *Journal of Geophysical Research*, 114(1), 1–10. <https://doi.org/10.1029/2007JG000644>
- Berg, A., Findell, K., Lintner, B., Giannini, A., Seneviratne, S. I., van den Hurk, B., et al. (2016). Land-atmosphere feedbacks amplify aridity increase over land under global warming. *Nature Climate Change*, 6, 869. <https://doi.org/10.1038/nclimate3029>
- Bonan, G. B., Lombardozzi, D. L., & Wieder, W. R. (2021). The signature of internal variability in the terrestrial carbon cycle. *Environmental Research Letters*, 16(3). <https://doi.org/10.1088/1748-9326/abd6a9>
- Bonan, G. B., Lombardozzi, D. L., Wieder, W. R., Oleson, K. W., Lawrence, D. M., Hoffman, F. M., & Collier, N. (2019). Model structure and climate data uncertainty in historical simulations of the terrestrial carbon cycle (1850–2014). *Global Biogeochemical Cycles*, 33(10), 1310–1326. <https://doi.org/10.1029/2019GB006175>
- Boysen, L. R., Brovkin, V., Pongratz, J., Lawrence, D. M., Lawrence, P., Vuichard, N., et al. (2020). Global climate response to idealized deforestation in CMIP6 models. *Biogeosciences*, 17(22), 5615–5638. <https://doi.org/10.5194/bg-17-5615-2020>



- Bradley, A. V., Gerard, F. F., Barbier, N., Weedon, G. P., Anderson, L. O., Huntingford, C., et al. (2011). Relationships between phenology, radiation, and precipitation in the Amazon region. *Global Change Biology*, 17(6), 2245–2260. <https://doi.org/10.1111/j.1365-2486.2011.02405.x>
- Brando, P. M., Goetz, S. J., Baccini, A., Nepstad, D. C., Beck, P. S. A., & Christman, M. C. (2010). Seasonal and interannual variability of climate and vegetation indices across the Amazon. *Proceedings of the National Academy of Sciences of the United States of America*, 107(33), 14685–14690. <https://doi.org/10.1073/pnas.0908741107>
- Brando, P. M., Nepstad, D. C., Davidson, E. A., Trumbore, S. E., Ray, D., & Camargo, P. (2008). Drought effects on litterfall, wood production and belowground carbon cycling in an Amazon forest: Results of a throughfall reduction experiment. *Philosophical Transactions of the Royal Society of London. Series B, Biological sciences*, 363(1498), 1839–1848. <https://doi.org/10.1098/rstb.2007.0031>
- Chadwick, R., Good, P., Martin, G., & Rowell, D. P. (2015). Large rainfall changes consistently projected over substantial areas of tropical land. *Nature Climate Change*, 6, 177. <https://doi.org/10.1038/nclimate2805>
- Chen, C. C., Lo, M. H., Im, E. S., Yu, J. Y., Liang, Y. C., Chen, W. T., et al. (2019). Thermodynamic and dynamic responses to deforestation in the Maritime Continent: A modeling study. *Journal of Climate*, 32(12), 3505–3527. <https://doi.org/10.1175/JCLI-D-18-0310.1>
- Cook, B. I., Mankin, J. S., Marvel, K., Williams, A. P., Smerdon, J. E., & Anchukaitis, K. J. (2020). Twenty-first century drought projections in the CMIP6 forcing scenarios. *Earth's Future*, 8(6). <https://doi.org/10.1029/2019EF001461>
- Corlett, R. T. (2016). The impacts of droughts in tropical forests. *Trends in Plant Science*, 21(7), 584–593. <https://doi.org/10.1016/j.tplants.2016.02.003>
- Doughty, C. E., & Goulden, M. L. (2008). Seasonal patterns of tropical forest leaf area index and CO<sub>2</sub> exchange. *Journal of Geophysical Research*, 113(G1). <https://doi.org/10.1029/2007JG000590>
- Duffy, P. B., Brando, P., Asner, G. P., & Field, C. B. (2015). Projections of future meteorological drought and wet periods in the Amazon. *Proceedings of the National Academy of Sciences*, 112(43), 13172–13177. <https://doi.org/10.1073/pnas.1421010112>
- Fearnside, P. M. (2018). Brazil's Amazonian forest carbon: The key to Southern Amazonia's significance for global climate. *Regional Environmental Change*, 18(1), 47–61. <https://doi.org/10.1007/s10113-016-1007-2>
- Fisher, R. A., Williams, M., Costada, A. L., Malhi, Y., Costada, R. F., Almeida, S., & Meir, P. (2007). The response of an Eastern Amazonian rain forest to drought stress: Results and modeling analyses from a throughfall exclusion experiment. *Global Change Biology*, 13(11), 2361–2378. <https://doi.org/10.1111/j.1365-2486.2007.01417.x>
- Flack-Prairie, S., Meir, P., Malhi, Y., Smallman, T. L., & Williams, M. (2019). The importance of physiological, structural, and trait responses to drought stress in driving spatial and temporal variation in GPP across Amazon forests. *Biogeosciences*, 16(22), 4463–4484. <https://doi.org/10.5194/bg-16-4463-2019>
- Friedlingstein, P., Jones, M. W., O'Sullivan, M., Andrew, R. M., Hauck, J., Peters, G. P., et al. (2019). Global carbon budget 2019. *Earth System Science Data*, 11(4), 1783–1838. <https://doi.org/10.5194/essd-11-1783-2019>
- Gatti, L. V., Gloor, M., Miller, J. B., Doughty, C. E., Malhi, Y., Domingues, L. G., et al. (2014). Drought sensitivity of Amazonian carbon balance revealed by atmospheric measurements. *Nature*, 506(7486), 76–80. <https://doi.org/10.1038/nature12957>
- Girardin, C. A. J., Malhi, Y., Doughty, C. E., Metcalfe, D. B., Meir, P., Aguila-Pasquel, J., et al. (2016). Seasonal trends of Amazonian rainforest phenology, net primary productivity, and carbon allocation. *Global Biogeochemical Cycles*, 30(5), 700–715. <https://doi.org/10.1002/2015GB005270>
- Green, J. K., Seneviratne, S. I., Berg, A. M., Findell, K. L., Hagemann, S., Lawrence, D. M., & Gentile, P. (2019). Large influence of soil moisture on long-term terrestrial carbon uptake. *Nature*, 565(7740), 476–479. <https://doi.org/10.1038/s41586-018-0848-x>
- Guan, K., Pan, M., Li, H., Wolf, A., Wu, J., Medvigy, D., et al. (2015). Photosynthetic seasonality of global tropical forests constrained by hydroclimate. *Nature Geoscience*, 8(4), 284–289. <https://doi.org/10.1038/ngeo2382>
- Harper, A., Baker, I. T., Denning, A. S., Randall, D. A., Dazlich, D., & Branson, M. (2014). Impact of evapotranspiration on dry season climate in the Amazon forest. *Journal of Climate*, 27(2), 574–591. <https://doi.org/10.1175/JCLI-D-13-00074.1>
- Huang, Y., Gerber, S., Huang, T., & Lichstein, J. W. (2016). Evaluating the drought response of CMIP5 models using global gross primary productivity, leaf area, precipitation, and soil moisture data. *Global Biogeochemical Cycles*, 30(12), 1827–1846. <https://doi.org/10.1002/2016GB005480>
- Humphrey, V., Berg, A., Ciais, P., Gentile, P., Jung, M., Reichstein, M., et al. (2021). Soil moisture-atmosphere feedback dominates land carbon uptake variability. *Nature*, 592(7852), 65–69. <https://doi.org/10.1038/s41586-021-03325-5>
- Janssen, T., Fleischer, K., Luyssaert, S., Naudts, K., & Dolman, H. (2020). Drought resistance increases from the individual to the ecosystem level in highly diverse Neotropical rain forest: A meta-analysis of leaf, tree and ecosystem responses to drought. *Biogeosciences Discussions*, 1–41. <https://doi.org/10.5194/bg-2019-497>
- Joetzer, E., Delire, C., Douville, H., Ciais, P., Decharme, B., Fisher, R., et al. (2014). Predicting the response of the Amazon rainforest to persistent drought conditions under current and future climates: A major challenge for global land surface models. *Geoscientific Model Development*, 7(6), 2933–2950. <https://doi.org/10.5194/gmd-7-2933-2014>
- Joetzer, E., Douville, H., Delire, C., & Ciais, P. (2013). Present-day and future Amazonian precipitation in global climate models: CMIP5 vs. CMIP3. *Climate Dynamics*, 41(11–12), 2921–2936. <https://doi.org/10.1007/s00382-012-1644-1>
- Jones, C., Robertson, E., Arora, V., Friedlingstein, P., Shevliakova, E., Bopp, L., et al. (2013). Twenty-first-century compatible CO<sub>2</sub> emissions and airborne fraction simulated by CMIP5 Earth System Models under four representative concentration pathways. *Journal of Climate*, 26(13), 4398–4413. <https://doi.org/10.1175/JCLI-D-12-00554.1>
- Kern, S. (2021). MODIS collection 6 global 8-daily LAI and FAPAR. <https://doi.org/10.25592/uhhfdm.8585>
- Kim, Y., Knox, R. G., Longo, M., Medvigy, D., Hutrya, L. R., Pyle, E. H., et al. (2012). Seasonal carbon dynamics and water fluxes in an Amazon rainforest. *Global Change Biology*, 18(4), 1322–1334. <https://doi.org/10.1111/j.1365-2486.2011.02629.x>
- Lejeune, Q., Davin, E. L., Guillod, B. P., & Seneviratne, S. I. (2015). Influence of Amazonian deforestation on the future evolution of regional surface fluxes, circulation, surface temperature, and precipitation. *Climate Dynamics*, 44(9–10), 2769–2786. <https://doi.org/10.1007/s00382-014-2203-8>
- Le Quéré, C., Andrew, R. M., Friedlingstein, P., Sitch, S., Hauck, J., Pongratz, J., et al. (2018). Global carbon budget 2018. *Earth System Science Data*, 10(4), 2141–2194. <https://doi.org/10.5194/essd-10-2141-2018>
- Lewis, S. L., Brando, P. M., Phillips, O. L., Van Der Heijden, G. M., & Nepstad, D. (2011). The 2010 Amazon drought. *Science*, 331(6017), 554. <https://doi.org/10.1126/science.1200807>
- Lin, Y.-H., Lo, M.-H., & Chou, C. (2015). Potential negative effects of groundwater dynamics on dry season convection in the Amazon River basin. *Climate Dynamics*. <https://doi.org/10.1007/s00382-015-2628-8>
- Lopes, A. P., Nelson, B. W., Wu, J., Alencastro Graça, P. M. L., Tavares, J. V., Prohaska, N., et al. (2016). Leaf flush drives dry season green-up of the Central Amazon. *Remote Sensing of Environment*, 182, 90–98. <https://doi.org/10.1016/j.rse.2016.05.009>

- Lorenz, R., Argüeso, D., Donat, M. G., Pitman, A. J., Van Den Hurk, B., Berg, A., et al. (2016). Influence of land-atmosphere feedbacks on temperature and precipitation extremes in the GLACE-CMIP5 ensemble. *Journal of Geophysical Research: Atmospheres*, 121(2), 607–623. <https://doi.org/10.1002/2015JD024053>
- Malhi, Y., Roberts, J. T., Betts, R. A., Killeen, T. J., Li, W., & Nobre, C. A. (2008). Climate change, deforestation, and the fate of the Amazon. *Science*, 319(5861), 169–172. <https://doi.org/10.1126/science.1146961>
- Manoli, G., Ivanov, V. Y., & Fatichi, S. (2018). Dry-season greening and water stress in Amazonia: The role of modeling leaf phenology. *Journal of Geophysical Research: Biogeosciences*, 123(6). <https://doi.org/10.1029/2017JG004282>
- Marengo, J. A., Nobre, C. A., Tomasella, J., Oyama, M. D., Oliveirade, G. S., Oliveirade, R., et al. (2008). The drought of Amazonia in 2005. *Journal of Climate*, 21(3), 495–516. <https://doi.org/10.1175/2007JCLI1600.1>
- Mauritsen, T., Bader, J., Becker, T., Behrens, J., Bittner, M., Brokopf, R., et al. (2019). Developments in the MPI-M Earth System Model version 1.2 (MPI-ESM1.2) and its response to increasing CO<sub>2</sub>. *Journal of Advances in Modeling Earth Systems*, 11(4), 998–1038. <https://doi.org/10.1029/2018MS001400>
- May, W., Rummukainen, M., Chérut, F., Hagemann, S., & Meier, A. (2017). Contributions of soil moisture interactions to future precipitation changes in the GLACE-CMIP5 experiment. *Climate Dynamics*, 49(5–6), 1681–1704. <https://doi.org/10.1007/s00382-016-3408-9>
- Meir, P., Mencuccini, M., Binks, O., Da Costa, A. L., Ferreira, L., & Rowland, L. (2018). Short-term effects of drought on tropical forest do not fully predict impacts of repeated or long-term drought: Gas exchange vs. growth. *Philosophical Transactions of the Royal Society B: Biological Sciences*, 373(1760). <https://doi.org/10.1098/rstb.2017.0311>
- Meir, P., Metcalfe, D. B., Costa, A. C., & Fisher, R. A. (2008). The fate of assimilated carbon during drought: Impacts on respiration in Amazon rainforests. *Philosophical Transactions of the Royal Society B: Biological Sciences*, 363(1498), 1849–1855. <https://doi.org/10.1098/rstb.2007.0021>
- Meir, P., Wood, T. E., Galbraith, D. R., Brando, P. M., Da Costa, A. C. L., Rowland, L., & Ferreira, L. V. (2015). Threshold responses to soil moisture deficit by trees and soil in tropical rain forests: Insights from field experiments. *BioScience*, 65(9), 882–892. <https://doi.org/10.1093/biosci/biv107>
- Munné-Bosch, S., & Alegre, L. (2004). Die and let live: Leaf senescence contributes to plant survival under drought stress. *Functional Plant Biology*, 31(3), 203. <https://doi.org/10.1071/FP03236>
- Myneni, R. B., Knyazikhin, Y., & Park, T. (2015). MOD15A2H MODIS/Terra Leaf Area Index/FPAR 8-Day 14 Global 500 m SIN Grid V006. <https://doi.org/10.5067/MODIS/MOD15A2H.006>
- Myneni, R. B., Yang, W., Nemani, R. R., Huete, A. R., Dickinson, R. E., Knyazikhin, Y., et al. (2007). Large seasonal swings in leaf area of Amazon rainforests. *Proceedings of the National Academy of Sciences of the United States of America*, 104(12), 4820–4823. <https://doi.org/10.1073/pnas.0611338104>
- Nabel, J. E. M. S., Naudts, K., & Pongratz, J. (2020). Accounting for forest age in the tile-based dynamic global vegetation model JSBACH4 (4.20p7; git feature/forests)—A land surface model for the ICON-ESM. *Geoscientific Model Development*, 13, 185–200. <https://doi.org/10.5194/gmd-13-185-2020>
- Nepstad, D. C., Moutinho, P., Dias-Filho, M. B., Davidson, E., Cardinot, G., Markewitz, D., et al. (2002). The effects of partial throughfall exclusion on canopy processes, aboveground production, and biogeochemistry of an Amazon forest. *Journal of Geophysical Research: Atmospheres*, 107(D20). LBA53-1–LBA53–18. <https://doi.org/10.1029/2001JD000360>
- Nobre, C. A., Sampaio, G., Borma, L. S., Castilla-Rubio, J. C., Silva, J. S., & Cardoso, M. (2016). Land-use and climate change risks in the Amazon and the need of a novel sustainable development paradigm. *Proceedings of the National Academy of Sciences of the United States of America*, 113(39), 10759–10768. <https://doi.org/10.1073/pnas.1605516113>
- Pan, Y., Birdsey, R. A., Fang, J., Houghton, R., Kauppi, P. E., Kurz, W. A., et al. (2011). A large and persistent carbon sink in the world's forests. *Science*, 333(6045), 988–993. <https://doi.org/10.1126/science.1201609>
- Patterson, K. A. (1990). *Global distribution of total and total-available soil water-holding capacities*. (M. Sc. thesis) (Vol. 119). Retrieved from <https://ci.nii.ac.jp/naid/10003485498/en/>
- Peano, D., Hemming, D., Materia, S., Delire, C., Fan, Y., Joetzier, E., et al. (2020). Plant phenology evaluation of CRESCENDO land surface models—Part I: Start and end of growing season. *Biogeosciences Discussions*, 1–36. <https://doi.org/10.5194/bg-2020-319>
- Phillips, O. L., Aragão, L. E. O. C., Lewis, S. L., Fisher, J. B., Lloyd, J., López-González, G., et al. (2009). Drought sensitivity of the Amazon rainforest. *Science*, 323(5919), 1344–1347. <https://doi.org/10.1126/science.1164033>
- Polle, A., Chen, S. L., Eckert, C., & Harfouche, A. (2019). Engineering drought resistance in forest trees. *Frontiers in Plant Science*, 9. <https://doi.org/10.3389/fpls.2018.01875>
- Powell, T. L., Galbraith, D. R., Christoffersen, B. O., Harper, A., Imbuzeiro, H. M. A., Rowland, L., et al. (2013). Confronting model predictions of carbon fluxes with measurements of Amazon forests subjected to experimental drought. *New Phytologist*, 200(2), 350–365. <https://doi.org/10.1111/nph.12390>
- Priestley, C. H. B., & Taylor, R. J. (1972). On the assessment of surface heat flux and evaporation using large-scale parameters. *Monthly Weather Review*, 100(2), 81–92. [https://doi.org/10.1175/1520-0493\(1972\)100<0081:OTAOSH>2.3.CO;2](https://doi.org/10.1175/1520-0493(1972)100<0081:OTAOSH>2.3.CO;2)
- Raczka, B., Dietze, M. C., Serbin, S. P., & Davis, K. J. (2018). What limits predictive certainty of long-term carbon uptake? *Journal of Geophysical Research: Biogeosciences*, 123(12), 3570–3588. <https://doi.org/10.1029/2018JG004504>
- Rayner, N. A., Parker, D. E., Horton, E. B., Folland, C. K., Alexander, L. V., Rowell, D. P., et al. (2003). Global analyses of sea surface temperature, sea ice, and night marine air temperature since the late nineteenth century. *Journal of Geophysical Research D: Atmospheres*, 108(14). <https://doi.org/10.1029/2002jd002670>
- Reick, C. H., Gayler, V., Goll, D., Hagemann, S., Heidkamp, M., & Nabel, J. E. M. S., et al. (2021). JSBACH 3—The land component of the MPI Earth System Model: Documentation of version 3.2. *Berichte zur Erdsystemforschung*, 240
- Restrepo-Coupe, N., Levine, N. M., Christoffersen, B. O., Albert, L. P., Wu, J., Costa, M. H., et al. (2017). Do dynamic global vegetation models capture the seasonality of carbon fluxes in the Amazon basin? A data-model intercomparison. *Global Change Biology*, 23(1), 191–208. <https://doi.org/10.1111/gcb.13442>
- Rowland, L., Harper, A., Christoffersen, B. O., Galbraith, D. R., Imbuzeiro, H. M., Powell, T. L., & Williams, M. (2015). Modeling climate change responses in tropical forests: Similar productivity estimates across five models, but different mechanisms and responses. *Geoscientific Model Development*, 8(4), 1097–1110. <https://doi.org/10.5194/gmd-8-1097-2015>
- Sitch, S., Friedlingstein, P., Gruber, N., Jones, S. D., Murray-Tortarolo, G., Ahlström, A., et al. (2015). Recent trends and drivers of regional sources and sinks of carbon dioxide. *Biogeosciences*, 12(3), 653–679. <https://doi.org/10.5194/bg-12-653-2015>
- Staal, A., Flores, B. M., Aguiar, A. P. D., Bosmans, J. H., Fetzer, I., & Tuinenburg, O. A. (2020). Feedback between drought and deforestation in the Amazon. *Environmental Research Letters*, 15(4). <https://doi.org/10.1088/1748-9326/ab738e>

- Tokarska, K. B., Arora, V. K., Gillett, N. P., Lehner, F., Rogelj, J., Schleussner, C. F., et al. (2020). Uncertainty in carbon budget estimates due to internal climate variability. *Environmental Research Letters*, 15(10). <https://doi.org/10.1088/1748-9326/abaf1b>
- Trugman, A. T., Medvigy, D., Mankin, J. S., & Anderegg, W. R. L. (2018). Soil moisture stress as a major driver of carbon cycle uncertainty. *Geophysical Research Letters*, 1–9. <https://doi.org/10.1029/2018GL078131>
- Vourlitis, G. L., De Souza Nogueira, J., De Almeida Lobo, F., Sendall, K. M., De Paulo, S. R., Antunes Dias, C. A., et al. (2008). Energy balance and canopy conductance of a tropical semi-deciduous forest of the Southern Amazon Basin. *Water Resources Research*, 44(3), 1–14. <https://doi.org/10.1029/2006WR005526>
- Wu, J., Albert, L. P., Lopes, A. P., Restrepo-Coupe, N., Hayek, M., Wiedemann, K. T., et al. (2016). Leaf development and demography explain photosynthetic seasonality in Amazon evergreen forests. *Science*, 351(6276), 972–976. <https://doi.org/10.1126/science.aad5068>
- Wu, J., Guan, K., Hayek, M., Restrepo-Coupe, N., Wiedemann, K. T., Xu, X., et al. (2017). Partitioning controls on Amazon forest photosynthesis between environmental and biotic factors at hourly to interannual timescales. *Global Change Biology*, 23, 1240–1257. <https://doi.org/10.1111/gcb.13509>
- Wu, J., Kobayashi, H., Stark, S. C., Meng, R., Guan, K., Tran, N. N., et al. (2018). Biological processes dominate seasonality of remotely sensed canopy greenness in an Amazon evergreen forest. *New Phytologist*, 217(4), 1507–1520. <https://doi.org/10.1111/nph.14939>
- Yang, Y., Saatchi, S. S., Xu, L., Yu, Y., Choi, S., Phillips, N., et al. (2018). Post-drought decline of the Amazon carbon sink. *Nature Communications*, 9(1), 3172. <https://doi.org/10.1038/s41467-018-05668-6>
- Yin, L., Fu, R., Shevliakova, E., & Dickinson, R. E. (2013). How well can CMIP5 simulate precipitation and its controlling processes over tropical South America? *Climate Dynamics*, 41(11–12), 3127–3143. <https://doi.org/10.1007/s00382-012-1582-y>
- Zemp, D. C., Schleussner, C. F., Barbosa, H. M., Hirota, M., Montade, V., Sampaio, G., & Rammig, A. (2017). Self-amplified Amazon forest loss due to vegetation-atmosphere feedbacks. *Nature Communications*, 8, 1–10. <https://doi.org/10.1038/ncomms14681>
- Zeng, N., Yoon, J. H., Marengo, J. A., Subramaniam, A., Nobre, C. A., Mariotti, A., & Neelin, J. D. (2008). Causes and impacts of the 2005 Amazon drought. *Environmental Research Letters*, 3(1). <https://doi.org/10.1088/1748-9326/3/1/014002>
- Zhou, S., Park Williams, A., Berg, A. M., Cook, B. I., Zhang, Y., Hagemann, S., & Gentile, P. (2019). Land-atmosphere feedbacks exacerbate concurrent soil drought and atmospheric aridity. *Proceedings of the National Academy of Sciences of the United States of America*, 116(38), 18848–18853. <https://doi.org/10.1073/pnas.1904955116>

## References From the Supporting Information

- Clapp, R. B., & Hornberger, G. M. (1978). Empirical equations for some soil hydraulic properties. *Water Resources Research*, 14(4), 601–604. <https://doi.org/10.1029/WR014i004p00601>
- Malhado, A. C., Costa, M. H., Limade, F. Z., Portilho, K. C., & Figueiredo, D. N. (2009). Seasonal leaf dynamics in an Amazonian tropical forest. *Forest Ecology and Management*, 258(7), 1161–1165. <https://doi.org/10.1016/j.foreco.2009.06.002>
- Poorter, H., Niinemets, Ü., Poorter, L., Wright, I. J., & Villar, R. (2009). Causes and consequences of variation in leaf mass per area (LMA): A meta-analysis. *New Phytologist*, 182(3), 565–588. <https://doi.org/10.1111/j.1469-8137.2009.02830.x>
- Weedon, G. P., Balsamo, G., Bellouin, N., Gomes, S., Best, M. J., & Viterbo, P. (2014). The WFDEI meteorological forcing data set: Watch forcing data methodology applied to era-interim reanalysis data. *Water Resources Research*, 50(9), 7505–7514. <https://doi.org/10.1002/2014WR015638>
- Weedon, G. P., Gomes, S., Viterbo, P., Shuttleworth, W. J., Blyth, E., Österle, H., et al. (2011). Creation of the WATCH forcing data and its use to assess global and regional reference crop evaporation over land during the twentieth century. *Journal of Hydrometeorology*, 12(5), 823–848. <https://doi.org/10.1175/2011JHM1369.1>
- Wu, J., Serbin, S. P., Xu, X., Albert, L. P., Chen, M., Meng, R., et al. (2017). The phenology of leaf quality and its within-canopy variation is essential for accurate modeling of photosynthesis in tropical evergreen forests. *Global Change Biology*, 23(11), 4814–4827. <https://doi.org/10.1111/gcb.13725>